MGNN: Graph Neural Networks Inspired by Distance Geometry Problem

Guanyu Cui
Renmin University of China
Beijing, China
cuiguanyu@ruc.edu.cn

Zhewei Wei*
Renmin University of China
Beijing, China
zhewei@ruc.edu.cn

ABSTRACT

Graph Neural Networks (GNNs) have emerged as a prominent research topic in the field of machine learning. Existing GNN models are commonly categorized into two types: spectral GNNs, which are designed based on polynomial graph filters, and spatial GNNs, which utilize a message-passing scheme as the foundation of the model. For the expressive power and universality of spectral GNNs, a natural approach is to improve the design of basis functions for better approximation ability. As for spatial GNNs, models like Graph Isomorphism Networks (GIN) analyze their expressive power based on Graph Isomorphism Tests. Recently, there have been attempts to establish connections between spatial GNNs and geometric concepts like curvature and cellular sheaves, as well as physical phenomena like oscillators. However, despite the recent progress, there is still a lack of comprehensive analysis regarding the universality of spatial GNNs from the perspectives of geometry and physics.

In this paper, we propose MetricGNN (MGNN), a spatial GNN model inspired by the congruent-insensitivity property [1] of classifiers in the classification phase of GNNs. We demonstrate that a GNN model is universal in the spatial domain if it can generate embedding matrices that are congruent to any given embedding matrix. This property is closely related to the Distance Geometry Problem (DGP). Since DGP is an NP-Hard combinatorial optimization problem, we propose optimizing an energy function derived from spring networks and the Multi-Dimensional Scaling (MDS) problem. This approach also allows our model to handle both homophilic and heterophilic graphs. Finally, we propose employing the iteration method to optimize our energy function. We extensively evaluate the effectiveness of our model through experiments conducted on both synthetic and real-world datasets. Our code is available at: https://github.com/GuanyuCui/MGNN.

*Zhewei Wei is the corresponding author. The work was partially done at Gaoling School of Artificial Intelligence, Peng Cheng Laboratory, Beijing Key Laboratory of Big Data Management and Analysis Methods and MOE Key Lab of Data Engineering and Knowledge Engineering.

[1]That is, they can produce identical outputs when given two congruent input matrices. Congruent matrices are defined as matrices where the distance between each pair of corresponding rows remains the same. Formally, for every pair of i and j, the equality $d(\boldsymbol{A}_{i:}, \boldsymbol{A}_{j:}) = d(\boldsymbol{B}_{i:}, \boldsymbol{B}_{j:})$ holds.

CCS CONCEPTS

• **Computing methodologies** → **Neural networks**; **Machine learning algorithms**.

KEYWORDS

graph neural networks, distance geometry problem, metric matrix

ACM Reference Format:
Guanyu Cui and Zhewei Wei. 2023. MGNN: Graph Neural Networks Inspired by Distance Geometry Problem. In *Proceedings of the 29th ACM SIGKDD Conference on Knowledge Discovery and Data Mining (KDD '23), August 6–10, 2023, Long Beach, CA, USA.* ACM, New York, NY, USA, 13 pages. https://doi.org/10.1145/3580305.3599431

1 INTRODUCTION

Graph Neural Networks. With the rapid growth of graph data, Graph Neural Networks (GNNs) have been widely used in many areas such as physics simulation [47], traffic forecasting [33], and recommendation systems [60, 65], etc.. A typical scheme of a GNN consists of following components:

- An embedding function $f_\theta(\cdot)$ which maps the original node feature matrix $\boldsymbol{X} \in \mathbb{R}^{n\times F}$ to an initial embedding matrix $\boldsymbol{Z}^{(0)}$. The linear layers and MLPs are commonly used both in spatial models, such as GCNII [9], and spectral models, such as ChebNet [14], BernNet [24], etc..
- A graph propagation / convolution module $GP(\boldsymbol{Z}; \boldsymbol{A})$ which propagates the hidden features $\boldsymbol{Z}$ on the graph with adjacency matrix $\boldsymbol{A}$. While spectral models are inspired by spectral graph theory, it is worth noting that the filter utilized in these models can also be implemented using the message passing method.
- An optional pooling or readout module $R(\boldsymbol{Z}^{(K)}; \boldsymbol{A})$ which extract features from the final embedding matrix $\boldsymbol{Z}^{(K)}$ for graph-level tasks.
- A final output function $g_\theta(\boldsymbol{Z}^{(K)})$ for classification or regression with the embeddings generated. The linear layers and MLPs are also commonly used.

We can refer to the initial two stages as the embedding phase of the GNN, while the subsequent stages can be referred to as the classification phase [2]. Figure 1 is an illustration of a typical scheme of GNNs.

Expressive Power and Universality of GNNs. There is a significant body of literature dedicated to exploring the expressive power and universality of GNNs. Notably, the GIN model [61] is the first to highlight the connection between the expressive power of GNNs

[2]Some regression tasks also use MLPs as their regression functions, we can also regard them as classification tasks.

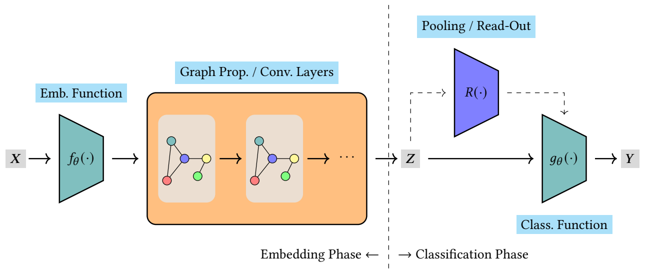

Figure 1: A typical scheme of GNNs.

and the Weisfeiler-Lehman graph isomorphism test. Furthermore, Chen et al. [10] establishes the equivalent relation between graph isomorphism test and function approximation on graphs. There are works trying to discuss the design of universal GNNs from the spectral perspective as well. For instance, Balcilar et al. [3] bridges the gap between spectral and spatial perspectives by reformulating various GNNs within a common framework. BernNet [24] proposes to use Bernstein basis to approximate arbitrary graph spectral filter, and Wang et al. [55] proves that linear GNNs can generate arbitrary graph signals, under some conditions regarding the graph Laplacian $\boldsymbol{L}$ and node features $\boldsymbol{X}$.

Our Contribution. In this paper, we discuss the universality of GNNs from a different geometric and physical perspective. Our contributions can be summarized as follows:

- Inspired by the congruent-insensitivity property of the classification phase of GNNs, we propose that a spatial-universal GNN should possess the capability to generate congruent embeddings with any embedding matrix produced by other GNNs.
- To generate congruent embeddings, we propose the MGNN model, which aims to minimize an energy function that carries physical meaning. We also discuss the relation of that objective function to the distance geometry problem, the multidimensional scaling problem, which provides strong theoretical backgrounds for our model.
- We propose to use the stationary point iteration method to optimize the objective function.
- We design experiments with synthetic and real-world graphs to show the effectiveness of the proposed MGNN model.

2 OTHER RELATED WORKS

In this section, we will list some other related works.

Distance Geometry and Graph Rigidity. Distance Geometry (DG) is a mathematical discipline that focuses on determining the spatial arrangement of points by utilizing given pairwise distance constraints as input. It has applications in various fields, including sensor network localization [4], and molecular conformation analysis [12], etc.. The core problem in DG is known as the following Distance Geometry Problem (DGP) [34, 35]:

Distance Geometry Problem (DGP)

Given an integer $d > 0$, a simple undirected graph $G = (V, E)$, and a symmetric non-negative metric matrix $\boldsymbol{M}$, decide whether there exists an embedding matrix $\boldsymbol{Z} \in \mathbb{R}^{|V| \times d}$, such that

$$\forall (i,j) \in E, \|\boldsymbol{Z}_{i:} - \boldsymbol{Z}_{j:}\| = \boldsymbol{M}_{ij}.$$

When the norm $\|\cdot\|$ is the Euclidean norm, this problem is also called Euclidean Distance Geometry Problem (EDGP).

Graph Rigidity refers to the property of a graph to maintain its shape or configuration when subjected to external forces. If we imagine connecting the nodes of a graph with bars, the graph is considered rigid if its shape remains unchanged regardless of the movements or repositioning of its nodes [1].

Geometric- and Physics-Inspired GNNs. There has been a growing interest in exploring the connections between GNNs and various geometric objects. For instance, [50] generalizes curvature for graphs and reveals the relation between over-squashing phenomenon and graph curvature. Furthermore, there are other works utilize gradient flow [16] and cellular sheaves on graphs [6] to design new GNN structures. Additionally, there has been research focusing on the connections between GNNs and physical concepts. For example, [46] explores the relation between GNNs and oscillators, while [58] investigates the potential energy concepts from particle physics in the context of GNNs.

Optimization Derived GNNs. Several works focus on deriving new GNNs from carefully designed optimization objectives (usually energy functions) or consolidating existing models into a unified optimization framework. For instance, works such as [39, 63] propose new GNN models based on the graph signal denoising objective function. This objective function can be formulated as the sum of an ℓ_2 regularization term and a Laplacian regression term:

$$\mathcal{L}(\boldsymbol{z}) = \|\boldsymbol{z} - \boldsymbol{x}_{\text{in}}\|_2^2 + \lambda \boldsymbol{z}^\top \boldsymbol{L} \boldsymbol{z}. \tag{1}$$

Subsequent works have extended and generalized the graph signal denoising optimization objective in various ways. For example, BernNet [24] generalizes the Laplacian matrix in the regression term to any positive semidefinite function of the Laplacian. ElasticGNN [38] introduces additional ℓ_1 and ℓ_{21} regularization terms into the objective function. ^{p}GNN [19] generalizes the Laplacian matrix to the p-Laplacian matrix, and ACMP-GNN [58] both modify the Laplacian matrix and replace the ℓ_2 regularization term with the double-well potential.

3 PRELIMINARIES

Notations for Matrices and Vectors. We use boldface uppercase letters such as $\boldsymbol{X}$ for matrices; while boldface lowercase characters such as $\boldsymbol{x}$ denote column vectors. For matrices, $\boldsymbol{X}_{i:}$ denotes the i-th row of $\boldsymbol{X}$, $\boldsymbol{X}_{:j}$ denotes the j-th column of $\boldsymbol{X}$, $\boldsymbol{X}_{ij}$ denotes the ij-th element of $\boldsymbol{X}$, and $\boldsymbol{X}^\top$ denotes the transposition of $\boldsymbol{X}$. Meanwhile, $\text{diag}(\boldsymbol{X})$ denotes the column vector that consists of all diagonal elements of $\boldsymbol{X}$, i.e., $\text{diag}(\boldsymbol{X})_i = \boldsymbol{X}_{ii}$ $(i = 1, 2, \cdots, n)$. For vectors, $\boldsymbol{x}_i$ denotes the i-th element of $\boldsymbol{x}$, whereas $\boldsymbol{x}^\top$ denotes the transposition of $\boldsymbol{x}$. And $\text{diag}(\boldsymbol{x})$ denotes the square matrix whose diagonal elements are $\boldsymbol{x}$, i.e., $\mathrm{diag}(\boldsymbol{x})_{ij} = \begin{cases} \boldsymbol{x}_i, & i = j \\ 0, & i \neq j \end{cases}$. The Hadamard product is the element-wise product of two matrices or vectors, i.e., $(\boldsymbol{X} \odot \boldsymbol{Y})_{ij} = \boldsymbol{X}_{ij}\boldsymbol{Y}_{ij}$, and $(\boldsymbol{x} \odot \boldsymbol{y})_i = \boldsymbol{x}_i\boldsymbol{y}_i$.

Notations From the Graph Theory. An (unweighted) graph G is a pair (V, E), where V is the node set and $E \subseteq V^2$ is the edge set. We always denote $|V|$ and $|E|$ as $n = |V|$ and $m = |E|$. Given an arbitrary order for the nodes, we may denote V as $\{1, 2, \cdots, n\}$, and use the adjacency matrix $\boldsymbol{A} \in \{0, 1\}^{n\times n}$ to represent the edges E, i.e., $\boldsymbol{A}_{ij} = 1$ if and only if edge $(i, j) \in E$, otherwise $\boldsymbol{A}_{ij} = 0$. Note that for an undirected graph, $(i, j) \in E \Leftrightarrow (j, i) \in E$, resulting in a symmetric $\boldsymbol{A}$. Unless otherwise noted, the graphs below are undirected. The neighborhood of node i is the set of nodes that share an edge with it, i.e., $\mathcal{N}(i) := \{j : (i, j) \in E\}$. The degree of node i is the number of nodes in its neighborhood, i.e., $d_i := |\mathcal{N}(i)| = |\{j : (i, j) \in E\}|$. And the degree matrix of graph is $\boldsymbol{D} := \mathrm{diag}((d_1, d_2, \cdots, d_n))$. The Laplacian of graph is defined as $\boldsymbol{L} := \boldsymbol{D} - \boldsymbol{A}$.

Concepts From the Graph Rigidity Theory. We list the definitions of *equivalent*, *congruent*, *rigid* and *globally rigid* in the graph rigidity theory [27]:

Definition 3.1 (Equivalent). Two node embedding matrices $\boldsymbol{Z}^{(1)}$ and $\boldsymbol{Z}^{(2)} \in \mathbb{R}^{n\times d}$ of a graph G are equivalent (denoted as $\boldsymbol{Z}_1 \equiv_E \boldsymbol{Z}_2$) if $\|\boldsymbol{Z}^{(1)}_{i:} - \boldsymbol{Z}^{(1)}_{j:}\|_2 = \|\boldsymbol{Z}^{(2)}_{i:} - \boldsymbol{Z}^{(2)}_{j:}\|_2$ for all $(i, j) \in E$.

Definition 3.2 (Congruent). Two node embedding matrices $\boldsymbol{Z}^{(1)}$ and $\boldsymbol{Z}^{(2)} \in \mathbb{R}^{n\times d}$ of a graph G are congruent (denoted as $\boldsymbol{Z}_1 \cong_{V^2} \boldsymbol{Z}_2$) if $\|\boldsymbol{Z}^{(1)}_{i:} - \boldsymbol{Z}^{(1)}_{j:}\|_2 = \|\boldsymbol{Z}^{(2)}_{i:} - \boldsymbol{Z}^{(2)}_{j:}\|_2$ for all $i, j \in V$.

Definition 3.3 (Globally Rigid). An embedding matrix $\boldsymbol{Z}$ of a graph G is globally rigid if all its equivalent embedding matrices $\boldsymbol{Z}'$ are also congruent to $\boldsymbol{Z}$.

Definition 3.4 (Rigid). An embedding matrix $\boldsymbol{Z}$ of a graph G is rigid if there exists $\varepsilon > 0$ such that every equivalent embedding $\boldsymbol{Z}'$ which satisfies $\|\boldsymbol{Z}_{v:} - \boldsymbol{Z}'_{v:}\|_2 < \varepsilon$ for all $v \in V$, is congruent to $\boldsymbol{Z}$. Or informally, all equivalent embeddings that can be obtained by **continuous** motion from $\boldsymbol{Z}$ are congruent to $\boldsymbol{Z}$.

It is important to note that the globally rigid condition is stronger than the rigid condition because not all rigid graphs are globally rigid. For instance, consider the following graph in $\mathbb{R}^2$. It is rigid because any continuous motion applied to it will lead to a set of equivalent embeddings. However, there exists an equivalent embedding that is not congruent.

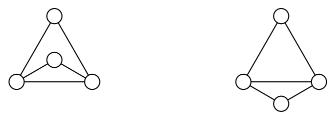

Figure 2: A rigid but not globally rigid graph (left) in $\mathbb{R}^2$, since it has an equivalent but not congruent embedding (right).

We also define the equivalent and congruent transformations and their corresponding groups for the convenience of discussion:

Definition 3.5 (Equivalent Transformation). Given a graph $G = (V, E)$ and an embedding matrix $\boldsymbol{Z}$, a reversible transformation $\mathcal{T} : \mathbb{R}^{n\times d} \to \mathbb{R}^{n\times d}$ is called E-equivalent if $\mathcal{T}(\boldsymbol{Z}) \equiv_E \boldsymbol{Z}$ always holds for all $\boldsymbol{Z} \in \mathbb{R}^{n\times d}$.

Definition 3.6 (Congruent Transformation). Given a graph $G = (V, E)$ and an embedding matrix $\boldsymbol{Z}$, a reversible transformation $\mathcal{T} : \mathbb{R}^{n\times d} \to \mathbb{R}^{n\times d}$ is called V^2-congruent if $\mathcal{T}(\boldsymbol{Z}) \cong_{V^2} \boldsymbol{Z}$ always holds for all $\boldsymbol{Z} \in \mathbb{R}^{n\times d}$.

It can be demonstrated straightforwardly that these two types of transformations constitute two groups, with transformation composition serving as the group operation. We denote them as $\mathrm{Iso}(n, d; E)$ and $\mathrm{Iso}(n, d; V^2)$, or simply as $\mathrm{Iso}(E)$ and $\mathrm{Iso}(V^2)$ when the matrix dimensions can be inferred from the context. We have the following Theorem that character the relation between these groups:

Theorem 3.7. $\mathrm{E}(d) \cong \mathrm{Iso}(n, d; V^2) \leq \mathrm{Iso}(n, d; E)$, *where* $\mathrm{E}(d)$ *is the d-dimensional Euclidean group, i.e., the group containing the composition of orthogonal and translation transformations;* $\cong$ *denotes the group isomorphism relation, and* $\leq$ *denotes the subgroup relation.*

The proof of this theorem can be found in Appendix A.

For the convenience of discussion, we also provide the definition of the metric matrix:

Definition 3.8 (The Metric Matrix of an Embedding Matrix). The metric matrix of an embedding matrix $\boldsymbol{Z} \in \mathbb{R}^{n\times d}$ is defined as a matrix containing all pairwise distances between the embedding vectors, i.e., $(\boldsymbol{M}_{\boldsymbol{Z}})_{ij} = \|\boldsymbol{Z}_{i:} - \boldsymbol{Z}_{j:}\|_2$. The equivalent form is

$$\boldsymbol{M}_{\boldsymbol{Z}} = \left(\mathrm{diag}(\boldsymbol{Z}\boldsymbol{Z}^\top)\mathbf{1}_n^\top + \mathbf{1}_n\mathrm{diag}(\boldsymbol{Z}\boldsymbol{Z}^\top)^\top - 2\boldsymbol{Z}\boldsymbol{Z}^\top\right)^{\odot\frac{1}{2}}, \quad (2)$$

where $\boldsymbol{X}^{\odot k}$ is the element-wise power of $\boldsymbol{X}$. We also define the mapping from an embedding matrix $\boldsymbol{Z}$ to its metric matrix $\boldsymbol{M}_{\boldsymbol{Z}}$ as $\boldsymbol{M}_{\boldsymbol{Z}} = M(\boldsymbol{Z})$.

4 MOTIVATION

Several studies have examined the expressive power of GNNs. Some of these works investigate the connection between message-passing GNNs and the Weisfeiler-Lehman (WL) graph isomorphism test, including [3, 40, 42, 61]. Other studies focus on the relationship between spectral GNNs and graph filters, as explored in research papers such as [5, 11, 24, 29, 55].

Recently, there has been a growing trend of exploring the relationships between GNNs and geometric objects such as curvature [50], gradient flow [16], and cellular sheaves on graphs [6]. Additionally, there is increasing interest in investigating the relationships between GNNs and physical objects such as oscillators [46] and potential energy in particle physics [58]. To the best of our knowledge, there has been no previous research that analyzes the universality of spatial GNNs in relation to the metric matrix of embeddings and the distance geometry problem. Our work will explore how to design spatial-universal GNNs from those aspects and will also reveal their tight connections to the graph rigidity, the multidimensional scaling problem, and the spring networks.

4.1 Sufficient Conditions of a Spatial-Universal GNN

Intuitively, we can observe that common classification modules in GNNs can yield identical predictions when given congruent embedding matrices. In other words, applying congruent transformations to the embedding matrix does not impact the accuracy of predictions. Formally, we can state the following theorem to capture this observation:

Theorem 4.1 (MLPs Are Congruent-Insensitive)**.** *Given two congruent embedding matrices Z_1 and Z_2, for any MLP_M (with bias)* [3] *, there always exists another MLP_N (also with bias) such that $\mathrm{MLP}_M(Z_1) = \mathrm{MLP}_N(Z_2)$. That is, they produce identical predictions with Z_1 and Z_2, respectively.*

The proof of this theorem can be found in Appendix B.

Now we try to define the concept of a spatial-universal GNN. Universality refers to a model's capability to approximate various other models. A widely recognized universal model is the Universal Turing Machine (UTM) [52], which was introduced by the mathematician and computer scientist Alan Turing. Similar to the idea of the Universal Turing Machine, which has the ability to simulate any Turing Machine (TM), we anticipate that a universal GNN U can "simulate" any given GNN A by generating identical predictions to those of A. Based on Theorem 4.1, we can infer that if a GNN U can generate an embedding matrix that is congruent to the one produced by any given GNN A during its embedding phase, then U is capable of generating identical predictions to those of A.

4.2 Metric Matrix as a Guide

Just like every programmable TM can function as a UTM, we can consider the metric matrix as the "program" or the guide to design a spatial-universal GNN. If a GNN U can generate an embedding matrix Z_U using the provided metric matrix $\boldsymbol{M} = M(Z_N)$ of any other GNN N, then U is capable of producing identical predictions to N[4]. Given the observation that two embedding matrices are congruent if and only if their metric matrices are identical, we can infer that Z_U is congruent to Z_N, indicating that U is capable of generating identical predictions to N. Consequently, we can refer to U as a spatial-universal GNN to a certain degree. An illustration of the concept of spatial-universal GNNs is presented in Figure 3.

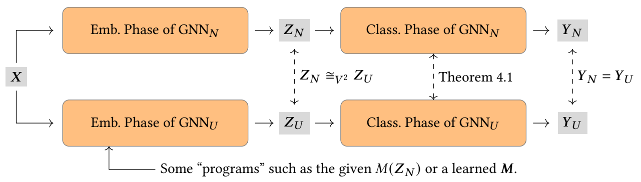
X
Emb. Phase of GNN_N
Z_N
Class. Phase of GNN_N
Y_N
$Z_N \cong_{V^2} Z_U$
Theorem 4.1
$Y_N = Y_U$
Emb. Phase of GNN_U
Z_U
Class. Phase of GNN_U
Y_U
Some "programs" such as the given $M(Z_N)$ or a learned $\boldsymbol{M}$.

Figure 3: The idea of the spatial-universal GNNs.

[3]MLP layers are formulated as $\boldsymbol{X}^{(k+1)} = \sigma\left(\boldsymbol{X}^{(k)}\boldsymbol{W}^{(k)} + \mathbf{1}(\boldsymbol{b}^{(k)})^\top\right)$. Linear layers can be regarded as the special cases of MLP layers when σ is the identity mapping.

[4]To be precise, suppose $\boldsymbol{Z}^* = \mathrm{GNN}_N(\boldsymbol{X};\boldsymbol{A})$, we can set $\boldsymbol{M}_{ij} = \|\boldsymbol{Z}^*_{i:} - \boldsymbol{Z}^*_{j:}\|_2$. In some cases, particularly for complex GNN models that we need to simulate, it may not be feasible to calculate the closed-form metric in advance. However, the theoretical existence of such metrics is still valid based on the aforementioned construction.

5 THE MGNN MODEL

5.1 The Optimization Objective

We have established that a GNN U can be regarded as a spatial-universal GNN if it is capable of producing an embedding matrix which is congruent to the embedding matrix generated by any other GNN. Consequently, we anticipate that spatial-universal GNNs have the potential to tackle the Distance Geometry Problem (DGP) [34] with $E = V^2$. Since the full metric matrix consists of all pairwise distances between the embedding vectors of nodes, computing the complete $\boldsymbol{M}$ matrix is a computationally intensive $O(n^2)$ operation. To alleviate the heavy computational burden, we propose relaxing the constraints by solely considering node pairs connected by edges. By doing so, computing the partial metric matrix becomes an $O(m)$ operation, which will lead to a local message-passing operation on the graph (see Section 5.3).

This adaptation has resulted in a reduction of expressive power from generating congruent embeddings to generating equivalent embeddings with the given $\boldsymbol{M}$. In the case of a globally rigid graph, where the pairwise distances between nodes connected by edges suffice to determine the "shape" of the embedding, all equivalent embeddings of such a graph are congruent. Therefore, this adaptation does not weaken the expressive power of the model in such cases. For a graph that is not globally rigid, its equivalent embeddings may not necessarily be congruent, and this adaptation weakens the expressive power in such cases. Unfortunately, testing the global rigidity of a graph is an NP-Hard problem [48], making it infeasible to test the global rigidity of the graph beforehand. Besides, not all non-negative symmetric matrices are valid metric matrices. For example, consider a triangle K_3 in $\mathbb{R}^2$, whose nodes are labelled as $V = \{1,2,3\}$. $\boldsymbol{M}^{(1)} = \begin{bmatrix} 0 & 3 & 4 \\ 3 & 0 & 5 \\ 5 & 4 & 0 \end{bmatrix}$ is a valid matrix, as there exists an embedding matrix $\boldsymbol{Z} = \begin{bmatrix} 0 & 0 & 4 \\ 0 & 3 & 0 \end{bmatrix}^\top$ satisfying the metric constraints. However, $\boldsymbol{M}^{(2)} = \begin{bmatrix} 0 & 1 & 1 \\ 1 & 0 & 3 \\ 1 & 3 & 0 \end{bmatrix}$ is not a valid matrix, since it does not satisfy the triangle inequality $\boldsymbol{M}_{1,2} + \boldsymbol{M}_{1,3} \geq \boldsymbol{M}_{2,3}$. Given that the DGP is NP-Hard [48], we can not effectively determine whether a given non-negative symmetric matrix is valid or not.

Hence, it becomes necessary to introduce an error-tolerant optimization objective for our model. We utilize the sum of squared estimate of errors (SSE) as the objective function:

$$\begin{aligned} E_p(\boldsymbol{Z};\boldsymbol{M},E) &= \frac{1}{2}\|\boldsymbol{A} \odot (M(\boldsymbol{Z}) - \boldsymbol{M})\|_F^2 \\ &= \sum_{(i,j)\in E} \frac{1}{2}\left(\|\boldsymbol{Z}_{i:} - \boldsymbol{Z}_{j:}\|_2 - \boldsymbol{M}_{ij}\right)^2. \end{aligned} \tag{3}$$

This optimization objective is originated from the raw Stress function σ_r in the Multidimensional Scaling (MDS) problem [8, 31]. Remarkably, this objective function also carries a physical interpretation. Spring network models, which are a special case of force-directed methods, have been employed in the field of graph drawing since the 1960s [18, 20, 28, 51, 53, 57]. These models have found applications in the biophysics and biochemistry domains for analyzing the properties of proteins [2, 22, 37]. Suppose that we have a spring network with the underlying graph $G = (V, E)$ in Figure 4. By considering the edges E as springs with characteristic constants $k_{ij} = 1$, the embedding matrix $\boldsymbol{Z}$ as the instantaneous positions of the nodes, and the metric matrix $\boldsymbol{M}$ as the relaxed lengths of the springs, the objective function $E_p(\boldsymbol{Z}; \boldsymbol{M}, E)$ represents the total elastic potential energy of the spring network.

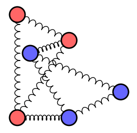
Figure 4: A spring network.

It is evident that the objective function E_p remains invariant under the group actions of $\mathrm{Iso}(E)$, or formally:

Theorem 5.1. *For any $\sigma \in \mathrm{Iso}(E)$, any matrix $\boldsymbol{M} \in \mathbb{R}^{n\times n}$, and any embedding $\boldsymbol{Z} \in \mathbb{R}^{n\times d}$, we have $E_p(\sigma(\boldsymbol{Z}); \boldsymbol{M}, E) = E_p(\boldsymbol{Z}; \boldsymbol{M}, E)$.*

The proof of this theorem can be found in Appendix C.

Several well-known spectral and spatial GNNs, such as GCN [29], SGC [59], APPNP [30], GCNII [9] and BernNet [24], utilize the normalized Laplacian matrix $\tilde{\boldsymbol{L}} = \boldsymbol{D}^{-1/2}\boldsymbol{L}\boldsymbol{D}^{-1/2} = \boldsymbol{I} - \boldsymbol{D}^{-1/2}\boldsymbol{A}\boldsymbol{D}^{-1/2}$ instead of the standard Laplacian matrix $\boldsymbol{L} = \boldsymbol{D} - \boldsymbol{A}$ to enhance the numerical stability. Following the convention established in related works, we also normalize our objective function by reparameterizing $\boldsymbol{Z}$ as $\boldsymbol{D}^{-1/2}\boldsymbol{Z}$, resulting in

$$\tilde{E}_p(\boldsymbol{Z}; \boldsymbol{M}, E) = E_p(\boldsymbol{D}^{-1/2}\boldsymbol{Z}; \boldsymbol{M}, E). \quad (4)$$

Furthermore, we add a trade-off regularization term to achieve the final optimization objective:

$$\mathcal{L}(\boldsymbol{Z}; \boldsymbol{Z}^{(0)}, \boldsymbol{M}, E) = (1-\alpha)\tilde{E}_p(\boldsymbol{Z}; \boldsymbol{M}, E) + \alpha\|\boldsymbol{Z} - \boldsymbol{Z}^{(0)}\|_F^2, \quad (5)$$

where $\boldsymbol{Z}^{(0)} = f_\theta(\boldsymbol{X})$ is the initial embedding matrix of node features (see the framework of the model in Section 5.3).

5.2 Design of the Metric Matrix

Another crucial aspect of our model is the design of the metric matrix. In this section, we will discuss various ways to design it.

Pre-Designed Metric Matrix $\boldsymbol{M}$. One straightforward approach to obtain the elements in $\boldsymbol{M}$ is to utilize a pre-designed metric matrix. For example, in certain scenarios like molecular conformation generation or graph drawing, if we possess prior knowledge about bond lengths or distances between nodes, we can directly assign the metric matrix for the MGNN model. Theoretically, we can also set the metric matrix according to the output embeddings of any given GNN. However, as it is hard to know the metric matrix in advance, this approach is only practical under some specific circumstances.

Learning Metric Matrix $\boldsymbol{M}$. A more general and reasonable approach is to learn the metric matrix from data. Intuitively, to differentiate between nodes, we aim to increase the distance between dissimilar nodes and reduce the distance between similar nodes. We can introduce a set of variables called edge attention, denoted as $\alpha_{ij} \in [-1, 1]$, associated with each edge to reflect the similarity between the two nodes connected by the edge. Indeed, when the value of α_{ij} approaches 1, it indicates that nodes i and j tend to belong to the same class. On the other hand, when α_{ij} approaches -1, it suggests that nodes i and j are more likely to belong to different classes. The design of the edge attention is inspired by research on heterophilic graphs, where nodes with different labels tend to be connected by edges [5, 11, 24, 43, 56, 62, 63, 66]. Additionally, it draws inspiration from signed graphs, where edges are labeled with either +1 or -1, indicating positive or negative associations [15, 23, 26]. We suggest employing the following commonly used attention mechanisms to obtain the edge attention α_{ij}:

- "concat": $\alpha_{ij} = \tanh\left(\boldsymbol{a}^\top\left[\boldsymbol{H}_{i:}^\top \| \boldsymbol{H}_{j:}^\top\right]\right)$;
- "bilinear": $\alpha_{ij} = \tanh\left(\boldsymbol{H}_{i:}\boldsymbol{W}\boldsymbol{H}_{j:}^\top\right)$.

The matrix $\boldsymbol{H} = \mathrm{MLP}(\boldsymbol{Z}^{(0)})$ consists of hidden representations learned from the initial node embeddings. Then we leverage these representations to learn the edge attention α_{ij}. Based on the meaning of α_{ij}, we can design the elements $\boldsymbol{M}_{ij}$ in the metric matrix. Specifically, as $\alpha_{ij} \to 1$, we desire $\boldsymbol{M}_{ij}$ to approach 0, and as $\alpha_{ij} \to -1$, we want $\boldsymbol{M}_{ij}$ to tend towards $+\infty$. One simple design that fulfills these conditions is to set $\boldsymbol{M}_{ij}$ as follows:

$$\boldsymbol{M}_{ij} = \frac{1-\alpha_{ij}}{1+\alpha_{ij}+\varepsilon}\|\boldsymbol{Z}_{i:}^{(0)} - \boldsymbol{Z}_{j:}^{(0)}\|_2, \quad (6)$$

where ε is a small positive number, and $\boldsymbol{Z}^{(0)}$ is the initial embedding matrix.

5.3 Solution and Framework

In this section, we will present the complete framework of the model.

Embedding. Following the standard scheme of GNNs, we first embed the raw node features into a d-dimensional latent space via an embedding function $\boldsymbol{Z}^{(0)} = f_\theta(\boldsymbol{X})$ to reduce the dimension. A linear layer

$$f_{\boldsymbol{W},\boldsymbol{b}}(\boldsymbol{X}) = \boldsymbol{X}\boldsymbol{W} + \boldsymbol{1}\boldsymbol{b}^\top \quad (7)$$

in linear GNNs or a two-layer MLP

$$f_{\boldsymbol{W}_1,\boldsymbol{W}_2,\boldsymbol{b}_1,\boldsymbol{b}_2}(\boldsymbol{X}) = \sigma(\sigma(\boldsymbol{X}\boldsymbol{W}_1 + \boldsymbol{1}\boldsymbol{b}_1^\top)\boldsymbol{W}_2 + \boldsymbol{1}\boldsymbol{b}_2^\top) \quad (8)$$

in spectral GNNs are all good choices for the embedding function.

Propagation. In this section, for formula conciseness, we use the notation $\tilde{\boldsymbol{X}}$ to represent $\boldsymbol{D}^{-1/2}\boldsymbol{X}\boldsymbol{D}^{-1/2}$ for any matrix $\boldsymbol{X}$.

We will design a graph propagation method which tries to minimize the objective function in Equation 5. Unfortunately, the objective function is generally non-convex when for some i, j, $\boldsymbol{M}_{ij} > \|\boldsymbol{Z}_{i:} - \boldsymbol{Z}_{j:}\|_2$, which means it may have multiple local minima, making it challenging to find the global minimum. Consequently, we can employ iterative methods such as gradient descent [31, 32] or stationary point iteration [21] introduced in [13] to optimize the objective function $E_p(\boldsymbol{Z}; \boldsymbol{M}, E)$. The gradient descent method leverages gradient information to iteratively update the embeddings until reaching a point with a near-zero gradient. This is quite similar to the idea of stationary point iteration method which uses the first order necessary condition $\nabla f = \boldsymbol{0}$ to derive an iteration equation. By employing the stationary point iteration method, we can derive a propagation equation that exhibits a similar form and maintains close connections to related works in the field. To begin, let us compute the gradient of the final optimization objective function with respect to the embedding $\boldsymbol{Z}$:

$$\frac{\partial \mathcal{L}}{\partial \boldsymbol{Z}} = 2(1-\alpha)\boldsymbol{D}^{-1/2}(\operatorname{diag}(\boldsymbol{S}\mathbf{1}) - \boldsymbol{S})\boldsymbol{D}^{-1/2}\boldsymbol{Z} + 2\alpha(\boldsymbol{Z} - \boldsymbol{Z}^{(0)}), \quad (9)$$

where $\boldsymbol{S} = \boldsymbol{A} - \boldsymbol{A} \odot \boldsymbol{M} \odot M(\boldsymbol{D}^{-1/2}\boldsymbol{Z})^{\odot -1}$. Setting the gradient of $\mathcal{L}$ to zero and rearranging the terms, we obtain the following equation:

$$\boldsymbol{Z} = (1-\alpha)\tilde{\boldsymbol{A}}\boldsymbol{Z} + (1-\alpha)\widetilde{\boldsymbol{L}_{\boldsymbol{H}}}\boldsymbol{Z} + \alpha \boldsymbol{Z}^{(0)}, \quad (10)$$

where $\boldsymbol{H} = \boldsymbol{A} \odot \boldsymbol{M} \odot M(\boldsymbol{D}^{-1/2}\boldsymbol{Z})^{\odot -1}$, and $\boldsymbol{L}_{\boldsymbol{H}} = \operatorname{diag}(\boldsymbol{H}\mathbf{1}) - \boldsymbol{H}$. The meaning of using the notation $\boldsymbol{L}_{\boldsymbol{H}}$ is that if we have a graph G whose adjacency matrix is $\boldsymbol{H}$, the Laplacian of G is $\boldsymbol{L}_{\boldsymbol{H}}$. We rewrite the equation as an iteration form, and substitute $1-\alpha$ with β in the second term to allow more flexibility. This leads us to the final propagation equation:

$$\boldsymbol{Z}^{(k+1)} = (1-\alpha)\tilde{\boldsymbol{A}}\boldsymbol{Z}^{(k)} + \beta\widetilde{\boldsymbol{L}_{\boldsymbol{H}}}\boldsymbol{Z}^{(k)} + \alpha \boldsymbol{Z}^{(0)}, \quad (11)$$

We can also derive the message-passing form of the propagation rule as follows:

$$\boldsymbol{Z}_{i:}^{(k+1)} = (1-\alpha)\sum_{j\in N(i)} \frac{\boldsymbol{Z}_{i:}^{(k)}}{\sqrt{d_i d_j}} + \beta \sum_{j\in N(i)} \frac{\boldsymbol{M}_{ij}\left(\boldsymbol{Z}_{i:}^{(k)} - \boldsymbol{Z}_{j:}^{(k)}\right)}{\sqrt{d_i d_j}\left\|\frac{\boldsymbol{Z}_{i:}^{(k)}}{\sqrt{d_i}} - \frac{\boldsymbol{Z}_{j:}^{(k)}}{\sqrt{d_j}}\right\|_2} + \alpha \boldsymbol{Z}_{i:}^{(0)}. \quad (12)$$

We may refer to the first term, $\tilde{\boldsymbol{A}}\boldsymbol{Z}^{(k)}$, in Equation 11 "topological message" since it aggregates the hidden features based on the graph topology. Similarly, we can name the second term, $\widetilde{\boldsymbol{L}_{\boldsymbol{H}}}\boldsymbol{Z}^{(k)}$, the "metric message" as it aggregates the hidden features according to the metric matrix. It is worth noting that this equation can be viewed as a generalization of the propagation equation in the APPNP model [30].

Optional Linear and Non-Linear Transformations. For applications where a pre-designed metric matrix is not available, such as node classification, we can incorporate linear and non-linear transformations into our MGNN model, similar to the approach used in the GCNII model [9]. Now we have the updating rule for tasks which need to learn metric matrix from data:

$$\boldsymbol{Z}^{(k+1)} = \sigma(((1-\alpha)\tilde{\boldsymbol{A}}\boldsymbol{Z}^{(k)} + \beta\widetilde{\boldsymbol{L}_{\boldsymbol{H}}}\boldsymbol{Z}^{(k)} + \alpha\boldsymbol{Z}^{(0)})(\gamma^{(k)}\boldsymbol{W}^{(k)} + (1-\gamma^{(k)})\boldsymbol{I})), \quad (13)$$

where $\gamma^{(k)}$ is set as in the GCNII model. That is, $\gamma^{(k)} = \log(1+\theta/k)$, and θ is a hyper-parameter. For applications where a pre-designed metric matrix is available in advance, such as graph drawing, we do not include additional linear and non-linear transformations in the propagation rule.

Classification. Finally, we map the hidden representation vector to the output dimension using a classification function $\boldsymbol{Y} = g_\theta(\boldsymbol{Z}^{(L)})$. We use a single-layer linear model

$$g_{\boldsymbol{W},\boldsymbol{b}}(\boldsymbol{Z}^{(L)}) = \boldsymbol{Z}^{(L)}\boldsymbol{W} + \mathbf{1}\boldsymbol{b}^\top \quad (14)$$

as the final classification function.

6 EXPERIMENTS

In this section, we conduct experiments on both synthetic and real-world graphs to evaluate the performance of our MGNN model. All experiments are conducted on a server with an Intel Xeon Silver 4114 CPU (2.20GHz), an Nvidia Quadro RTX 8000 GPU (48GB) and 1TB of RAM.

6.1 Arranging Nodes with the Given Metric Matrices

To verify that our MGNN model can arrange the nodes with the given metric matrix correctly, we perform experiments on synthetic stochastic block model graphs.

Datasets. We randomly generate two stochastic block model (SBM) graphs: one homophilic and one heterophilic. Each graph comprises 4 blocks, with 50 nodes in each block. In the homophilic graph, the probability of intra-block edges is 0.3, while the probability of inter-class edges is 0.05. In the heterophilic graph, the probabilities are 0.05 and 0.2 for intra-block and inter-class edges, respectively. The node features in each block are sampled from four 2-dimensional Gaussian distributions, with parameters ($\boldsymbol{\mu} = [0,0]^\top, \Sigma = \boldsymbol{I}$), ($\boldsymbol{\mu} = [1,0]^\top, \Sigma = \boldsymbol{I}$), ($\boldsymbol{\mu} = [0,1]^\top, \Sigma = \boldsymbol{I}$), ($\boldsymbol{\mu} = [1,1]^\top, \Sigma = \boldsymbol{I}$).

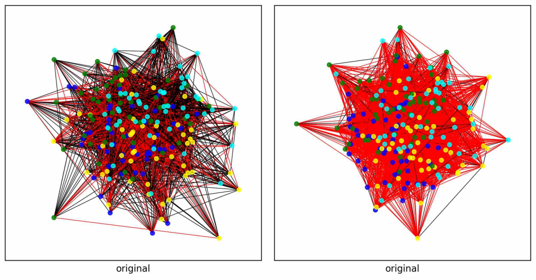

Figure 5: Generated homophilic (left) and heterophilic (right) graphs. Black edges are intra-class, while red edges are inter-class.

Settings and Results. We first generate two graphs as described above and visualize them in Figure 5. Next, we assign metric matrices $\boldsymbol{M}$ to the two graphs. Specifically, for nodes i and j belonging to the same block, $\boldsymbol{M}_{ij} = 0$, while for nodes in different blocks, $\boldsymbol{M}_{ij} = 5$. We propagate the node features through 8 MGNN propagation layers, using parameters $\alpha = 0.05$ and $\beta = 0.5$. After each round of propagation, we visualize the results. The results are visualized in Figure 6 and 7. Based on the results, we can confirm that our MGNN model aims to separate the four blocks. Moreover, for the homophilic graph, our MGNN model can arrange the nodes with the given metric matrix correctly. This is because the presence of homophilic edges adds convexity to our objective function, whereas heterophilic edges have the opposite effect, and it is known that convex functions are easier to optimize.

Compare MGNN with SGC and APPNP Layers. Additionally, we provide visualizations of the results obtained from the SGC layers (refer to Figure 8 and Figure 9 in Appendix D) and APPNP layers (refer to Figure 10 and Figure 11 in Appendix D) for the two synthetic graphs mentioned earlier. The results indicate that as we stack SGC layers, the embeddings of the nodes tend to converge towards a linear subspace, which will make the embedding vectors difficult to

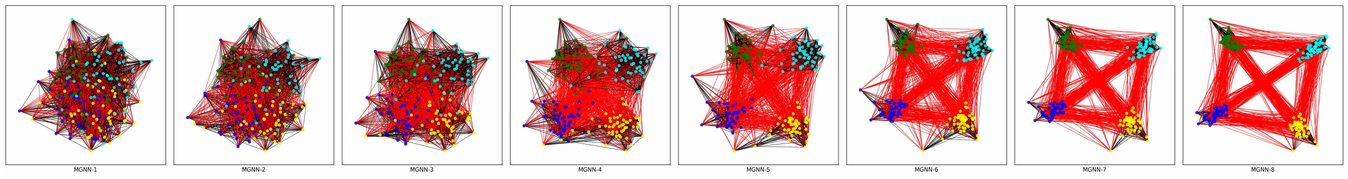

Figure 6: The results of the homophilic SBM graph of MGNN layers.

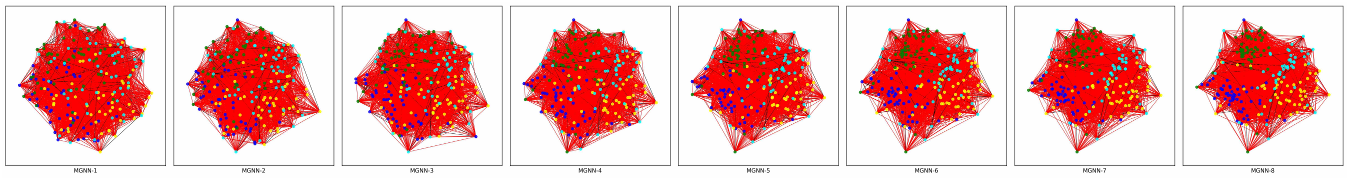

Figure 7: The results of the heterophilic SBM graph of MGNN layers.

classify. Furthermore, we can conclude that while stacking APPNP layers does not exhibit the same phenomenon as described above, the APPNP model is unable to arrange the nodes in accordance with the metric matrix as the MGNN layers.

6.2 Supervised Node Classification

To assess the real-world performance of our MGNN model, we conduct node-classification experiments and compare it with other models.

Datasets. As for the datasets, we carefully select many well-known benchmark graphs including the citation networks Cora, CiteSeer, PubMed from [64]; the CoraFull dataset from [7]; the coauthor networks CS and Physics from [49]; the WebKB networks Cornell, Texas and Wisconsin from [43]; the Wikipedia networks Chameleon and Squirrel from [45]; the actor co-occurrence network Actor from [43]; the WikiCS dataset from [41]; and the ogbn-arxiv dataset from [25]. We download and preprocess all datasets using either the PyTorch Geometric Library [17] or the official OGB package [25]. The basic statistics of the datasets, including the number of nodes, number of edges, number of features, number of classes, and the edge homophily (as defined in [66]) denoted as $\mathcal{H}(G, Y)$, are summarized in Table 1. The datasets encompass a wide range, from small graphs with approximately 200 nodes and 600 edges, to large graphs with around 170,000 nodes and over 2 million edges. Among these datasets, there are highly homophilic graphs with edge homophily values exceeding 0.9, as well as heterophilic graphs exhibiting homophily values below 0.1.

Methods. To demonstrate the effectiveness of the design of our MGNN model, we have selected various baseline models, including non-graph models, spectral GNNs, and spatial (non-spectral) GNN models. For the **non-graph models**, we have chosen the one-layer linear layer model (with bias) and the two-layer MLP model as our baselines. For the **spectral GNNs**, we have chosen the GCN model [29], the SGC model [59], and the APPNP model [30]. For the **spatial (non-spectral) GNNs**, we have selected the PointNet model [44], the GAT model [54], the GIN model [61], the GCNII model [9], the ^{p}GNN model [19], and the LINKX model [36].

Table 1: The statistics of the datasets.

Dataset	#Nodes	#Edges[1]	#Features	#Classes	$\mathcal{H}(G, Y)$
Cora	2,708	10,556	1,433	7	0.81
CiteSeer	3,327	9,104	3,703	6	0.74
PubMed	19,717	88,648	500	3	0.80
CoraFull	19,793	126,842	8,710	70	0.57
CS	18,333	163,788	6,805	15	0.81
Physics	34,493	495,924	8,415	5	0.93
Cornell	183	557	1,703	5	0.13
Texas	183	574	1,703	5	0.09
Wisconsin	251	916	1,703	5	0.19
Chameleon	2,277	62,792	2,325	5	0.23
Squirrel	5,201	396,846	2,089	5	0.22
Actor	7,600	53,411	932	5	0.22
WikiCS	11,701	431,726	300	10	0.65
ogbn-arxiv	169,343	2,315,598	128	40	0.65

[1] We first transform directed graphs to undirected ones, then count the total number of pairs (i, j) in the edge sets for each dataset.

Efficiency of the Models. In this part, we will analyze the total number of trainable parameters and the time complexity of the forward pass for each model. We denote F as the number of features, representing the input dimension of the dataset. Similarly, c represents the number of classes, which indicates the output dimension of the dataset. We will use d to represent the hidden dimension, and L to denote the number of convolution layers or propagation depth. Meanwhile, suppose that a graph G has $n = |V|$ nodes and has $m = |E|$ edges.

For the one-layer linear model ($Y = \boldsymbol{X}\boldsymbol{W}_{F\times c} + \mathbf{1}\boldsymbol{b}_c^\top$), it has $O(Fc)$ trainable parameters, and its forward pass has a time complexity of $O(nFc)$. Regarding the L-layer MLP, each layer operates similarly to a linear layer, with the addition of a non-linear activation function. Consequently, each MLP layer possesses $O(\text{dim\_in} \times \text{dim\_out})$ trainable parameters, and the forward pass requires a time complexity of $O(n \times \text{dim\_in} \times \text{dim\_out})$.

The cases of the GNNs are complicated, so we first divide them into three phases and then analyze them individually.

- Embedding Phase: In the GCN, GAT and the GIN model, the embedding layers serve as their initial layers for dimension reduction. Consequently, they have $O(Fd)$ parameters ($O(Fd+d^2) = O(Fd)$ for GIN, as it utilizes a two-layer MLP as the update function), and their forward pass has a time complexity of $O(mF + nFd)$ (the $O(mF)$ portion accounts for the graph propagation operation, as explained below). In the case of the MGNN$_{\text{Linear}}$ model, the embedding function is implemented as a linear layer, which contains $O(Fd)$ trainable parameters and has a forward time complexity of $O(nFd)$. For the PointNet model, the APPNP model, the GCNII model, and the MGNN$_{\text{MLP}}$ model, their embedding function consists of a two-layer MLP. This MLP comprises $O(Fd+d^2) = O(Fd)$ trainable parameters and has a forward time complexity of $O(nFd + nd^2) = O(nFd)$. Regarding the ^{p}GNN model, its embedding function is a one-layer MLP, which possesses $O(Fd)$ parameters and has a forward time complexity of $O(nFd)$.
- Propagation / Convolution Phase: For message-passing GNNs (GNNs excluding the LINKX model), their propagation rules are $\boldsymbol{Z}_{i:}^{(k+1)} = \text{UPDATE}(\boldsymbol{Z}_{i:}^{(k)}, \text{AGG}_{j \in N(i)}\text{MSG}(\boldsymbol{Z}_{i:}^{(k)}, \boldsymbol{Z}_{j:}^{(k)}))$. These rules do not involve any trainable parameters and have a time complexity of $\sum_{i \in V} d_i d = O(md)$, assuming that $\text{MSG}(\boldsymbol{Z}_{i:}^{(k)}, \boldsymbol{Z}_{j:}^{(k)})$ takes $O(d)$ time. For GCN, GAT, GIN, GCNII, PointNet, and our MGNN models, their convolution modules incorporate linear transformations, resulting in $O(d^2)$ parameters and an overall time complexity of $O(nd^2)$ per layer. In the case of GAT, each layer introduces an additional $O(d)$ parameters to learn the attention.
- Classification Phase: For the GCN, GAT and the GIN model, the classification layers are their last layers. They possess $O(dc)$ ($O(d^2+dc)$ for GIN) parameters, and their forward time complexity is $O(md + ndc)$ ($O(md + nd^2 + ndc)$ for GIN). For other message-passing GNNs, their classification function is implemented as a linear layer, which has $O(dc)$ ($O(Fc)$ for SGC) parameters and $O(ndc)$ ($O(nFc)$ for SGC) forward time complexity.
- Other Modules: The LINKX model is not a normal message-passing GNN. Its structure is as follows:

$$\begin{aligned} \boldsymbol{H_A} &= \text{MLP}_{\boldsymbol{A}}(\boldsymbol{A}), \boldsymbol{H_X} = \text{MLP}_{\boldsymbol{X}}(\boldsymbol{X}), \\ \boldsymbol{H} &= \sigma([\boldsymbol{H_A} \| \boldsymbol{H_X}]\boldsymbol{W} + \boldsymbol{H_A} + \boldsymbol{H_X}), \\ \boldsymbol{Y} &= \text{MLP}_f(\boldsymbol{H}). \end{aligned} \tag{15}$$

We denote $L_{\boldsymbol{A}}$ as the number of layers in MLP$_{\boldsymbol{A}}$, $L_{\boldsymbol{X}}$ as the number of layers in MLP$_{\boldsymbol{X}}$, L_f as the number of layers in MLP$_f$, and $L = L_{\boldsymbol{A}} + L_{\boldsymbol{X}} + L_f$ represents the total number of layers. The MLP$_{\boldsymbol{A}}$ has $O(nd + d^2 L_{\boldsymbol{A}})$ parameters and the time complexity is $O(md + nd^2 L_{\boldsymbol{A}})$. Note that the first layer, $\boldsymbol{H}_{\boldsymbol{A}}^{(1)} = \sigma(\boldsymbol{A}\boldsymbol{W}_0 + \boldsymbol{1}\boldsymbol{b}_0^\top)$, can be implemented with sparse matrix multiplication, resulting in a time complexity of $O(md)$. Similarly, the MLP$_{\boldsymbol{X}}$ has $O(Fd + d^2 L_{\boldsymbol{X}})$ parameters and the time complexity is $O(nFd + nd^2 L_{\boldsymbol{X}})$. The computation of $\boldsymbol{H}$ requires $O(d^2)$ parameters and takes $O(nd^2)$ time. Lastly, the MLP$_f$ has $O(d^2 L_f + dc)$ trainable parameters, and its forward time complexity is $O(nd^2 L_f + ndc)$. In the case of the PointNet model, there is a position generation layer that comprises a two-layer MLP. This layer possesses $O(d^2)$ trainable parameters, and the forward time complexity is $O(nd^2)$. As for our MGNN model, it incorporates a metric layer consisting of a two-layer MLP and an attention module. The metric layer has $O(d^2)$ trainable parameters, and its time complexity is $O(md^2)$.

We summarize the total parameters of each model in Table 2, and their forward pass time complexity in Table 3.

Table 2: The total number of trainable parameters of each model.

	Embedding	Prop./Conv./Hidden	Classification	Others	Total
Linear	–	–	$O(Fc)$	–	$O(Fc)$
MLP	$O(Fd)$	$O(d^2L)$	$O(dc)$	–	$O(d(F+dL+c))$
GCN	$O(Fd)$	$O(d^2L)$	$O(dc)$	–	$O(d(F+dL+c))$
SGC	0	0	$O(Fc)$	–	$O(Fc)$
APPNP	$O(Fd)$	0	$O(dc)$	–	$O(d(F+d+c))$
PointNet	$O(Fd)$	$O(d^2L)$	$O(dc)$	$O(d^2)$	$O(d(F+dL+c))$
GAT	$O(Fd)$	$O(d^2L)$	$O(dc)$	–	$O(d(F+dL+c))$
GIN	$O(Fd)$	$O(d^2L)$	$O(d^2+dc)$	–	$O(d(F+dL+c))$
GCNII	$O(Fd)$	$O(d^2L)$	$O(dc)$	–	$O(d(F+dL+c))$
^{p}GNN	$O(Fd)$	0	$O(dc)$	–	$O(d(F+c))$
MGNN$_{\text{Linear}}$ MGNN$_{\text{MLP}}$	$O(Fd)$	$O(d^2L)$	$O(dc)$	$O(d^2)$	$O(d(F+dL+c))$

	MLP$_{\boldsymbol{A}}$	MLP$_{\boldsymbol{X}}$	Computing $\boldsymbol{H}$	MLP$_f$	Total
LINKX	$O(nd+d^2L_{\boldsymbol{A}})$	$O(Fd+d^2L_{\boldsymbol{X}})$	$O(d^2)$	$O(d^2L_f+dc)$	$O(d(dL+n+F+c))$

Table 3: The time complexity of each model.

	Embedding	Prop./Conv./Hidden	Classification	Others	Total
Linear	–	–	$O(nFc)$	–	$O(nFc)$
MLP	$O(nFd)$	$O(nd^2L)$	$O(ndc)$	–	$O(nd(F+dL+c))$
GCN	$O(mF+nFd)$	$O((md+nd^2)L)$	$O(md+ndc)$	–	$O(md(F+dL+c))$
SGC	–	$O(mFL)$	$O(nFc)$	–	$O(mF(L+c))$
APPNP	$O(nFd)$	$O(mdL)$	$O(ndc)$	–	$O(nd(F+d+c)+mdL)$
PointNet	$O(mF+nFd)$	$O((md+nd^2)L)$	$O(md+ndc)$	$O(nd^2)$	$O(md(F+dL+c))$
GAT	$O(mF+nFd)$	$O((md+nd^2)L)$	$O(md+ndc)$	–	$O(md(F+dL+c))$
GIN	$O(mF+nFd)$	$O((md+nd^2)L)$	$O(md+nd^2+ndc)$	–	$O(md(F+dL+c))$
GCNII	$O(nFd)$	$O((md+nd^2)L)$	$O(ndc)$	–	$O(nd(F+d+c)+md^2L)$
^{p}GNN	$O(nFd)$	$O(mdL)$	$O(ndc)$	–	$O(nd(F+c)+mdL)$
MGNN$_{\text{Linear}}$ MGNN$_{\text{MLP}}$	$O(nFd)$	$O((md+nd^2)L)$	$O(ndc)$	$O(md^2)$	$O(nd(F+d+c)+md^2L)$

	MLP$_{\boldsymbol{A}}$	MLP$_{\boldsymbol{X}}$	Computing $\boldsymbol{H}$	MLP$_f$	Total
LINKX	$O(md+nd^2L_{\boldsymbol{A}})$	$O(nFd+nd^2L_{\boldsymbol{X}})$	$O(nd^2)$	$O(nd^2L_f+ndc)$	$O(d(ndL+m+nF+nc))$

Settings and Results. For all datasets except ogbn-arxiv, we generate 10 random splits with a consistent train/valid/test ratio of 60%/20%/20%. For the ogbn-arxiv dataset, we generate 10 random splits using the `get_idx_split()` function provided by the official package. We set the hidden units to 64 for all datasets. We then tune the hyper-parameters 100 times for each model on each dataset using the TPESampler from the optuna package. The ranges of the hyper-parameters are listed below:

- `learning_rate` for all models: {1e-3, 5e-3, 1e-2, 5e-2};
- `weight_decay` for all models: {0.0, 1e-5, 5e-5, 1e-4, 5e-4, 1e-3, 5e-3, 1e-2};
- `dropout` for all models: {0.0, 0.1, 0.3, 0.5};
- `num_layers` for all models: {2, 4, 8};
- `alpha` for APPNP, GCNII and MGNN: {0.00, 0.01, $\cdots$, 0.99, 1.00};
- `beta` for MGNN: {0.00, 0.01, $\cdots$, 0.99, 1.00};

Table 4: The results (accuracy with standard deviation) of the supervised node classification experiments. Boldface results indicate the best model on each dataset, and underlined results are second best models.

	Non-Graph		Spectral			Spatial (Non-Spectral)						MGNN
	Linear	MLP	GCN	SGC	APPNP	PointNet	GAT	GIN	GCNII	^{p}GNN	LINKX	
Cora	$76.09_{\pm 1.55}$	$76.11_{\pm 1.58}$	$88.25_{\pm 1.09}$	$88.34_{\pm 1.41}$	$\mathbf{89.30_{\pm 1.45}}$	$84.43_{\pm 1.94}$	$88.71_{\pm 0.89}$	$85.76_{\pm 1.18}$	$88.52_{\pm 1.40}$	$88.78_{\pm 1.20}$	$82.82_{\pm 1.96}$	$\underline{89.04_{\pm 1.20}}$
CiteSeer	$71.11_{\pm 1.81}$	$73.25_{\pm 1.16}$	$77.10_{\pm 1.12}$	$\underline{77.47_{\pm 1.42}}$	$76.80_{\pm 1.10}$	$72.83_{\pm 1.38}$	$76.44_{\pm 1.19}$	$72.83_{\pm 1.47}$	$77.05_{\pm 0.78}$	$77.28_{\pm 0.88}$	$71.79_{\pm 1.55}$	$\mathbf{78.08_{\pm 1.50}}$
PubMed	$87.06_{\pm 0.67}$	$88.21_{\pm 0.46}$	$89.07_{\pm 0.42}$	$87.59_{\pm 0.54}$	$89.75_{\pm 0.47}$	$89.18_{\pm 0.38}$	$87.77_{\pm 0.67}$	$87.15_{\pm 0.54}$	$\underline{90.24_{\pm 0.55}}$	$89.79_{\pm 0.38}$	$86.77_{\pm 0.59}$	$\mathbf{90.37_{\pm 0.47}}$
CoraFull	$60.55_{\pm 0.76}$	$61.61_{\pm 0.56}$	$71.86_{\pm 0.75}$	$71.86_{\pm 0.70}$	$71.88_{\pm 0.75}$	$63.32_{\pm 1.02}$	$70.65_{\pm 0.86}$	$67.11_{\pm 0.46}$	$71.09_{\pm 0.72}$	$\underline{72.36_{\pm 0.58}}$	$63.57_{\pm 0.55}$	$\mathbf{72.42_{\pm 0.69}}$
CS	$94.51_{\pm 0.32}$	$94.89_{\pm 0.23}$	$93.77_{\pm 0.37}$	$94.10_{\pm 0.40}$	$95.91_{\pm 0.23}$	$93.13_{\pm 0.42}$	$93.25_{\pm 0.31}$	$91.81_{\pm 0.34}$	$\underline{95.98_{\pm 0.22}}$	$95.83_{\pm 0.23}$	$95.06_{\pm 0.24}$	$\mathbf{96.01_{\pm 0.16}}$
Physics	$95.92_{\pm 0.15}$	$96.01_{\pm 0.26}$	$96.46_{\pm 0.25}$	OOM	$\underline{97.14_{\pm 0.21}}$	$96.37_{\pm 0.27}$	$96.47_{\pm 0.21}$	$94.66_{\pm 2.04}$	$97.10_{\pm 0.21}$	$96.93_{\pm 0.10}$	$96.87_{\pm 0.16}$	$\mathbf{97.15_{\pm 0.15}}$
Cornell	$\underline{78.65_{\pm 2.82}}$	$75.95_{\pm 4.43}$	$50.27_{\pm 6.86}$	$53.51_{\pm 4.32}$	$77.84_{\pm 6.49}$	$71.08_{\pm 5.93}$	$50.27_{\pm 7.66}$	$49.46_{\pm 7.46}$	$76.76_{\pm 7.76}$	$77.30_{\pm 8.22}$	$71.08_{\pm 12.09}$	$\mathbf{81.89_{\pm 6.29}}$
Texas	$81.35_{\pm 4.90}$	$83.78_{\pm 7.55}$	$61.08_{\pm 8.65}$	$56.22_{\pm 6.37}$	$86.76_{\pm 1.46}$	$82.16_{\pm 6.30}$	$61.08_{\pm 5.57}$	$64.05_{\pm 4.20}$	$\underline{88.65_{\pm 4.95}}$	$85.14_{\pm 5.16}$	$84.32_{\pm 5.24}$	$\mathbf{90.00_{\pm 2.72}}$
Wisconsin	$86.20_{\pm 3.63}$	$\mathbf{88.80_{\pm 2.40}}$	$55.80_{\pm 5.83}$	$58.00_{\pm 4.29}$	$86.00_{\pm 3.10}$	$81.60_{\pm 3.98}$	$56.40_{\pm 5.99}$	$57.20_{\pm 6.82}$	$88.20_{\pm 4.14}$	$85.40_{\pm 3.58}$	$82.00_{\pm 3.10}$	$\underline{88.40_{\pm 3.44}}$
Chameleon	$50.77_{\pm 2.07}$	$50.75_{\pm 2.13}$	$\underline{69.21_{\pm 2.08}}$	$67.12_{\pm 2.17}$	$67.85_{\pm 2.65}$	$63.76_{\pm 2.52}$	$66.97_{\pm 2.45}$	$46.73_{\pm 13.51}$	$67.56_{\pm 1.18}$	$69.19_{\pm 1.57}$	$67.47_{\pm 1.62}$	$\mathbf{72.37_{\pm 2.25}}$
Squirrel	$35.76_{\pm 1.05}$	$35.79_{\pm 1.65}$	$55.43_{\pm 2.05}$	$52.18_{\pm 1.49}$	$54.60_{\pm 1.88}$	$47.39_{\pm 8.31}$	$\underline{55.68_{\pm 2.81}}$	$20.96_{\pm 2.08}$	$53.88_{\pm 2.77}$	$51.61_{\pm 1.28}$	$\mathbf{57.86_{\pm 1.17}}$	$54.45_{\pm 1.85}$
Actor	$36.16_{\pm 0.75}$	$37.67_{\pm 1.60}$	$30.42_{\pm 1.58}$	$30.14_{\pm 1.18}$	$36.98_{\pm 1.28}$	$36.41_{\pm 1.23}$	$29.22_{\pm 0.94}$	$26.09_{\pm 1.75}$	$\underline{37.75_{\pm 1.23}}$	$36.47_{\pm 1.07}$	$35.00_{\pm 2.11}$	$\mathbf{38.36_{\pm 1.46}}$
WikiCS	$78.74_{\pm 0.57}$	$79.85_{\pm 0.69}$	$84.02_{\pm 0.61}$	$83.47_{\pm 0.83}$	$84.88_{\pm 0.55}$	$84.09_{\pm 0.86}$	$83.82_{\pm 0.73}$	$66.08_{\pm 22.77}$	$\underline{85.09_{\pm 0.71}}$	$84.41_{\pm 0.46}$	$84.13_{\pm 0.56}$	$\mathbf{85.09_{\pm 0.59}}$
ogbn-arxiv	$52.80_{\pm 0.19}$	$53.81_{\pm 0.23}$	$70.48_{\pm 0.18}$	$68.77_{\pm 0.06}$	$70.50_{\pm 0.11}$	$69.89_{\pm 0.59}$	$\underline{71.04_{\pm 0.27}}$	$66.60_{\pm 0.53}$	$\mathbf{71.48_{\pm 0.21}}$	$68.50_{\pm 0.17}$	$59.28_{\pm 2.22}$	$70.73_{\pm 0.17}$
Avg. Rank	9.21	7.86	6.79	7.69	3.50	7.86	7.57	10.50	3.50	4.36	7.29	1.57

- `theta` for GCNII and MGNN: {0.5, 1.0, 1.5};
- `mu` for ^{p}GNN: {0.00, 0.01, $\cdots$, 0.99, 1.00};
- `p` for ^{p}GNN: {0.5, 1.0, 1.5, 2.0};
- `initial`: for MGNN: {'Linear', 'MLP'};
- `attention` for MGNN: {'concat', 'bilinear'}.

We train each model for a maximum of 1500 epochs, with early stopping set to 100, on each dataset and report the results after hyper-tuning. The results of the supervised node classification experiments are presented in Table 4. We report the mean accuracy and the standard deviation based on 10 random splits generated as previously described. Our MGNN model generally performs well across all datasets, and outperforms all baselines in 10 out of 14 datasets. We also include the average rank of each model across all datasets. Our MGNN model achieves an average rank of 1.57, which is the highest among all models.

Ablation. Comparing the convolution rule of GCNII,

$$Z^{(k+1)} = \sigma(((1-\alpha)\tilde{A}Z^{(k)} + \alpha Z^{(0)})(\gamma^{(k)}W^{(k)} + (1-\gamma^{(k)})I)), \tag{16}$$

with that of our MGNN model (Equation 13), we can conclude that our MGNN model is a generalization of the GCNII model. In other words, the GCNII model can be considered as an ablation study of the MGNN model.

6.3 Graph Regression

To demonstrate the overall effectiveness of our MGNN model in graph regression tasks, we conducted experiments using the GCN model, GAT model, GIN model, PointNet model, and our MGNN model on the ZINC-subset dataset. Due to space constraints, we provide the detailed experiment settings in Appendix E. A summary of the results can be found in Table 5.

Table 5: The results of the graph regression experiments.

GCN	GAT	GIN	PointNet	MGNN
$0.6143_{\pm 0.0200}$	$0.6458_{\pm 0.0647}$	$\mathbf{0.4410_{\pm 0.0065}}$	$0.5293_{\pm 0.0138}$	$\underline{0.4751_{\pm 0.0112}}$

7 CONCLUSION

In this paper, we draw inspiration from the fact that typical classifiers, such as linear layers and MLPs, are not sensitive to congruent transformations. Based on this, we discuss the sufficient conditions for a spatial-universal GNN. To strike a balance between efficiency and expressive power, we propose a more relaxed model called MGNN. The optimization objective of MGNN is primarily focused on minimizing the raw stress arising from the distance geometry problem and the multidimensional scaling problem. We conducted extensive experiments on both synthetic datasets and real-world datasets. In the experiments involving the arrangement of nodes based on a given metric matrix, we observed that our MGNN model strives to separate blocks of nodes, particularly in the case of homophilic graphs. Furthermore, in node classification experiments, our MGNN model demonstrated superior performance in real-world applications. We hope that our model will provide new insights into spatial GNNs and inspire further explorations in this area.

ACKNOWLEDGMENTS

This research was supported in part by National Natural Science Foundation of China (No. U2241212, No. 61972401, No. 61932001, No. 61832017), by the major key project of PCL (PCL2021A12), by Beijing Natural Science Foundation (No. 4222028), by Beijing Outstanding Young Scientist Program No.BJJWZYJH012019100020098, by Alibaba Group through Alibaba Innovative Research Program, and by Huawei-Renmin University joint program on Information Retrieval. We also wish to acknowledge the support provided by Engineering Research Center of Next-Generation Intelligent Search and Recommendation, Ministry of Education. Additionally, we acknowledge the support from Intelligent Social Governance Interdisciplinary Platform, Major Innovation & Planning Interdisciplinary Platform for the "Double-First Class" Initiative, Public Policy and Decision-making Research Lab, Public Computing Cloud, Renmin University of China.

REFERENCES

[1] Abdo Y Alfakih. 2007. On dimensional rigidity of bar-and-joint frameworks. *Discrete applied mathematics* 155, 10 (2007), 1244–1253.

[2] Romain Amyot, Yuichi Togashi, and Holger Flechsig. 2019. Analyzing fluctuation properties in protein elastic networks with sequence-specific and distance-dependent interactions. *Biomolecules* 9, 10 (2019), 549.

[3] Muhammet Balcilar, Guillaume Renton, Pierre Héroux, Benoit Gaüzère, Sébastien Adam, and Paul Honeine. 2021. Analyzing the Expressive Power of Graph Neural Networks in a Spectral Perspective. In *9th International Conference on Learning Representations, ICLR 2021, Virtual Event, Austria, May 3-7, 2021.* OpenReview.net. https://openreview.net/forum?id=-qh0M9XWxnv

[4] Pratik Biswas, Tzu-Chen Lian, Ta-Chung Wang, and Yinyu Ye. 2006. Semidefinite programming based algorithms for sensor network localization. *ACM Transactions on Sensor Networks (TOSN)* 2, 2 (2006), 188–220.

[5] Deyu Bo, Xiao Wang, Chuan Shi, and Huawei Shen. 2021. Beyond Low-frequency Information in Graph Convolutional Networks. In *Thirty-Fifth AAAI Conference on Artificial Intelligence, AAAI 2021, Thirty-Third Conference on Innovative Applications of Artificial Intelligence, IAAI 2021, The Eleventh Symposium on Educational Advances in Artificial Intelligence, EAAI 2021, Virtual Event, February 2-9, 2021.* AAAI Press, 3950–3957. https://ojs.aaai.org/index.php/AAAI/article/view/16514

[6] Cristian Bodnar, Francesco Di Giovanni, Benjamin Paul Chamberlain, Pietro Liò, and Michael M. Bronstein. 2022. Neural Sheaf Diffusion: A Topological Perspective on Heterophily and Oversmoothing in GNNs. In *Advances in Neural Information Processing Systems*, Alice H. Oh, Alekh Agarwal, Danielle Belgrave, and Kyunghyun Cho (Eds.).

[7] Aleksandar Bojchevski and Stephan Günnemann. 2018. Deep Gaussian Embedding of Graphs: Unsupervised Inductive Learning via Ranking. In *6th International Conference on Learning Representations, ICLR 2018, Vancouver, BC, Canada, April 30 - May 3, 2018, Conference Track Proceedings.* OpenReview.net. https://openreview.net/forum?id=r1ZdKJ-0W

[8] Ingwer Borg and Patrick JF Groenen. 2005. *Modern multidimensional scaling: Theory and applications.* Springer Science & Business Media.

[9] Ming Chen, Zhewei Wei, Zengfeng Huang, Bolin Ding, and Yaliang Li. 2020. Simple and Deep Graph Convolutional Networks. In *Proceedings of the 37th International Conference on Machine Learning, ICML 2020, 13-18 July 2020, Virtual Event (Proceedings of Machine Learning Research, Vol. 119).* PMLR, 1725–1735. http://proceedings.mlr.press/v119/chen20v.html

[10] Zhengdao Chen, Soledad Villar, Lei Chen, and Joan Bruna. 2019. On the equivalence between graph isomorphism testing and function approximation with GNNs. In *Advances in Neural Information Processing Systems 32: Annual Conference on Neural Information Processing Systems 2019, NeurIPS 2019, December 8-14, 2019, Vancouver, BC, Canada.* 15868–15876.

[11] Eli Chien, Jianhao Peng, Pan Li, and Olgica Milenkovic. 2021. Adaptive Universal Generalized PageRank Graph Neural Network. In *9th International Conference on Learning Representations, ICLR 2021, Virtual Event, Austria, May 3-7, 2021.* OpenReview.net. https://openreview.net/forum?id=n6jl7fLxrP

[12] Gordon M Crippen, Timothy F Havel, et al. 1988. *Distance geometry and molecular conformation.* Vol. 74. Research Studies Press Taunton.

[13] Jan De Leeuw. 2005. Applications of convex analysis to multidimensional scaling. (2005).

[14] Michaël Defferrard, Xavier Bresson, and Pierre Vandergheynst. 2016. Convolutional Neural Networks on Graphs with Fast Localized Spectral Filtering. In *Advances in Neural Information Processing Systems 29: Annual Conference on Neural Information Processing Systems 2016, December 5-10, 2016, Barcelona, Spain*, Daniel D. Lee, Masashi Sugiyama, Ulrike von Luxburg, Isabelle Guyon, and Roman Garnett (Eds.). 3837–3845. https://proceedings.neurips.cc/paper/2016/hash/04df4d434d481c5bb723be1b6df1ee65-Abstract.html

[15] Tyler Derr, Yao Ma, and Jiliang Tang. 2018. Signed Graph Convolutional Networks. In *IEEE International Conference on Data Mining, ICDM 2018, Singapore, November 17-20, 2018.* IEEE Computer Society, 929–934. https://doi.org/10.1109/ICDM.2018.00113

[16] Francesco Di Giovanni, James Rowbottom, Benjamin P. Chamberlain, Thomas Markovich, and Michael M. Bronstein. 2022. Graph Neural Networks as Gradient Flows. https://arxiv.org/abs/2206.10991

[17] Matthias Fey and Jan E. Lenssen. 2019. Fast Graph Representation Learning with PyTorch Geometric. In *ICLR Workshop on Representation Learning on Graphs and Manifolds.*

[18] Thomas MJ Fruchterman and Edward M Reingold. 1991. Graph drawing by force-directed placement. *Software: Practice and experience* 21, 11 (1991), 1129–1164.

[19] Guoji Fu, Peilin Zhao, and Yatao Bian. 2022. p-Laplacian Based Graph Neural Networks. In *International Conference on Machine Learning, ICML 2022, 17-23 July 2022, Baltimore, Maryland, USA (Proceedings of Machine Learning Research, Vol. 162)*, Kamalika Chaudhuri, Stefanie Jegelka, Le Song, Csaba Szepesvári, Gang Niu, and Sivan Sabato (Eds.). PMLR, 6878–6917. https://proceedings.mlr.press/v162/fu22e.html

[20] Emden R Gansner, Yehuda Koren, and Stephen North. 2004. Graph drawing by stress majorization. In *International Symposium on Graph Drawing.* Springer, 239–250.

[21] Louis Guttman. 1968. A general nonmetric technique for finding the smallest coordinate space for a configuration of points. *Psychometrika* 33 (1968), 469–506.

[22] Turkan Haliloglu, Ivet Bahar, and Burak Erman. 1997. Gaussian Dynamics of Folded Proteins. *Phys. Rev. Lett.* 79 (Oct 1997), 3090–3093. Issue 16.

[23] Frank Harary. 1953. On the notion of balance of a signed graph. *Michigan Mathematical Journal* 2, 2 (1953), 143 – 146.

[24] Mingguo He, Zhewei Wei, Zengfeng Huang, and Hongteng Xu. 2021. BernNet: Learning Arbitrary Graph Spectral Filters via Bernstein Approximation. In *Advances in Neural Information Processing Systems.*

[25] Weihua Hu, Matthias Fey, Marinka Zitnik, Yuxiao Dong, Hongyu Ren, Bowen Liu, Michele Catasta, and Jure Leskovec. 2020. Open graph benchmark: Datasets for machine learning on graphs. *Advances in neural information processing systems* 33 (2020), 22118–22133.

[26] Junjie Huang, Huawei Shen, Liang Hou, and Xueqi Cheng. 2019. Signed Graph Attention Networks. In *Artificial Neural Networks and Machine Learning - ICANN 2019 - 28th International Conference on Artificial Neural Networks, Munich, Germany, September 17-19, 2019, Proceedings - Workshop and Special Sessions (Lecture Notes in Computer Science, Vol. 11731)*, Igor V. Tetko, Vera Kurková, Pavel Karpov, and Fabian J. Theis (Eds.). Springer, 566–577. https://doi.org/10.1007/978-3-030-30493-5_53

[27] Bill Jackson. 2007. Notes on the Rigidity of Graphs.

[28] Tomihisa Kamada and Satoru Kawai. 1989. An algorithm for drawing general undirected graphs. *Inform. Process. Lett.* 31, 1 (1989), 7–15.

[29] Thomas N. Kipf and Max Welling. 2017. Semi-Supervised Classification with Graph Convolutional Networks. In *5th International Conference on Learning Representations, ICLR 2017, Toulon, France, April 24-26, 2017, Conference Track Proceedings.* OpenReview.net. https://openreview.net/forum?id=SJU4ayYgl

[30] Johannes Klicpera, Aleksandar Bojchevski, and Stephan Günnemann. 2019. Predict then Propagate: Graph Neural Networks meet Personalized PageRank. In *7th International Conference on Learning Representations, ICLR 2019, New Orleans, LA, USA, May 6-9, 2019.* OpenReview.net. https://openreview.net/forum?id=H1gL-2A9Ym

[31] Joseph B Kruskal. 1964. Multidimensional scaling by optimizing goodness of fit to a nonmetric hypothesis. *Psychometrika* 29, 1 (1964), 1–27.

[32] Joseph B Kruskal. 1964. Nonmetric multidimensional scaling: a numerical method. *Psychometrika* 29, 2 (1964), 115–129.

[33] Yaguang Li, Rose Yu, Cyrus Shahabi, and Yan Liu. 2018. Diffusion Convolutional Recurrent Neural Network: Data-Driven Traffic Forecasting. In *6th International Conference on Learning Representations, ICLR 2018, Vancouver, BC, Canada, April 30 - May 3, 2018, Conference Track Proceedings.* OpenReview.net. https://openreview.net/forum?id=SJiHXGWAZ

[34] Leo Liberti and Carlile Lavor. 2017. *Euclidean Distance Geometry: An Introduction.* Springer International Publishing.

[35] Leo Liberti, Carlile Lavor, Nelson Maculan, and Antonio Mucherino. 2014. Euclidean distance geometry and applications. *SIAM review* 56, 1 (2014), 3–69.

[36] Derek Lim, Felix Hohne, Xiuyu Li, Sijia Linda Huang, Vaishnavi Gupta, Omkar Bhalerao, and Ser Nam Lim. 2021. Large scale learning on non-homophilous graphs: New benchmarks and strong simple methods. *Advances in Neural Information Processing Systems* 34 (2021), 20887–20902.

[37] Tu-Liang Lin and Guang Song. 2009. Generalized spring tensor models for protein fluctuation dynamics and conformation changes. In *2009 IEEE International Conference on Bioinformatics and Biomedicine Workshop.* 136–143.

[38] Xiaorui Liu, Wei Jin, Yao Ma, Yaxin Li, Hua Liu, Yiqi Wang, Ming Yan, and Jiliang Tang. 2021. Elastic Graph Neural Networks. In *Proceedings of the 38th International Conference on Machine Learning, ICML 2021, 18-24 July 2021, Virtual Event (Proceedings of Machine Learning Research, Vol. 139)*, Marina Meila and Tong Zhang (Eds.). PMLR, 6837–6849. http://proceedings.mlr.press/v139/liu21k.html

[39] Yao Ma, Xiaorui Liu, Tong Zhao, Yozen Liu, Jiliang Tang, and Neil Shah. 2021. A Unified View on Graph Neural Networks as Graph Signal Denoising. In *CIKM '21: The 30th ACM International Conference on Information and Knowledge Management, Virtual Event, Queensland, Australia, November 1 - 5, 2021*, Gianluca Demartini, Guido Zuccon, J. Shane Culpepper, Zi Huang, and Hanghang Tong (Eds.). ACM, 1202–1211. https://doi.org/10.1145/3459637.3482225

[40] Haggai Maron, Heli Ben-Hamu, Hadar Serviansky, and Yaron Lipman. 2019. Provably Powerful Graph Networks. In *Advances in Neural Information Processing Systems 32: Annual Conference on Neural Information Processing Systems 2019, NeurIPS 2019, December 8-14, 2019, Vancouver, BC, Canada*, Hanna M. Wallach, Hugo Larochelle, Alina Beygelzimer, Florence d'Alché-Buc, Emily B. Fox, and Roman Garnett (Eds.). 2153–2164. https://proceedings.neurips.cc/paper/2019/hash/bb04af0f7ecaee4aae62035497da1387-Abstract.html

[41] Péter Mernyei and Catalina Cangea. 2020. Wiki-CS: A Wikipedia-Based Benchmark for Graph Neural Networks. *CoRR* abs/2007.02901 (2020). arXiv:2007.02901 https://arxiv.org/abs/2007.02901

[42] Christopher Morris, Martin Ritzert, Matthias Fey, William L. Hamilton, Jan Eric Lenssen, Gaurav Rattan, and Martin Grohe. 2019. Weisfeiler and Leman Go

Neural: Higher-Order Graph Neural Networks. In *The Thirty-Third AAAI Conference on Artificial Intelligence, AAAI 2019, The Thirty-First Innovative Applications of Artificial Intelligence Conference, IAAI 2019, The Ninth AAAI Symposium on Educational Advances in Artificial Intelligence, EAAI 2019, Honolulu, Hawaii, USA, January 27 - February 1, 2019*. AAAI Press, 4602–4609. https://doi.org/10.1609/aaai.v33i01.33014602

[43] Hongbin Pei, Bingzhe Wei, Kevin Chen-Chuan Chang, Yu Lei, and Bo Yang. 2020. Geom-GCN: Geometric Graph Convolutional Networks. In *8th International Conference on Learning Representations, ICLR 2020, Addis Ababa, Ethiopia, April 26-30, 2020*. OpenReview.net. https://openreview.net/forum?id=S1e2agrFvS

[44] Charles Ruizhongtai Qi, Hao Su, Kaichun Mo, and Leonidas J. Guibas. 2017. PointNet: Deep Learning on Point Sets for 3D Classification and Segmentation. In *2017 IEEE Conference on Computer Vision and Pattern Recognition, CVPR 2017, Honolulu, HI, USA, July 21-26, 2017*. IEEE Computer Society, 77–85. https://doi.org/10.1109/CVPR.2017.16

[45] Benedek Rozemberczki, Carl Allen, and Rik Sarkar. 2021. Multi-Scale attributed node embedding. *J. Complex Networks* 9, 2 (2021). https://doi.org/10.1093/comnet/cnab014

[46] T. Konstantin Rusch, Ben Chamberlain, James Rowbottom, Siddhartha Mishra, and Michael M. Bronstein. 2022. Graph-Coupled Oscillator Networks. In *International Conference on Machine Learning, ICML 2022, 17-23 July 2022, Baltimore, Maryland, USA (Proceedings of Machine Learning Research, Vol. 162)*, Kamalika Chaudhuri, Stefanie Jegelka, Le Song, Csaba Szepesvári, Gang Niu, and Sivan Sabato (Eds.). PMLR, 18888–18909. https://proceedings.mlr.press/v162/rusch22a.html

[47] Alvaro Sanchez-Gonzalez, Jonathan Godwin, Tobias Pfaff, Rex Ying, Jure Leskovec, and Peter W. Battaglia. 2020. Learning to Simulate Complex Physics with Graph Networks. In *Proceedings of the 37th International Conference on Machine Learning, ICML 2020, 13-18 July 2020, Virtual Event (Proceedings of Machine Learning Research, Vol. 119)*. PMLR, 8459–8468. http://proceedings.mlr.press/v119/sanchez-gonzalez20a.html

[48] James B. Saxes. 1979. *Embeddability of Weighted Graphs in k-Space is Strongly NP-hard.* Technical Report. Carnegie Mellon University, USA.

[49] Oleksandr Shchur, Maximilian Mumme, Aleksandar Bojchevski, and Stephan Günnemann. 2018. Pitfalls of Graph Neural Network Evaluation. *CoRR* abs/1811.05868 (2018). arXiv:1811.05868 http://arxiv.org/abs/1811.05868

[50] Jake Topping, Francesco Di Giovanni, Benjamin Paul Chamberlain, Xiaowen Dong, and Michael M. Bronstein. 2022. Understanding over-squashing and bottlenecks on graphs via curvature. In *The Tenth International Conference on Learning Representations, ICLR 2022, Virtual Event, April 25-29, 2022*. OpenReview.net. https://openreview.net/forum?id=7UmjRGzp-A

[51] Daniel Tunkelang. 1994. *A Practical Approach to Drawing Undirected Graphs.* Technical Report. Carnegie Mellon University, USA.

[52] Alan Mathison Turing et al. 1936. On computable numbers, with an application to the Entscheidungsproblem. *J. of Math* 58, 345-363 (1936), 5.

[53] William T. Tutte. 1963. How to Draw a Graph. *Proceedings of The London Mathematical Society* 13 (1963), 743–767.

[54] Petar Velickovic, Guillem Cucurull, Arantxa Casanova, Adriana Romero, Pietro Liò, and Yoshua Bengio. 2018. Graph Attention Networks. In *6th International Conference on Learning Representations, ICLR 2018, Vancouver, BC, Canada, April 30 - May 3, 2018, Conference Track Proceedings*. OpenReview.net. https://openreview.net/forum?id=rJXMpikCZ

[55] Xiyuan Wang and Muhan Zhang. 2022. How Powerful are Spectral Graph Neural Networks. In *International Conference on Machine Learning, ICML 2022, 17-23 July 2022, Baltimore, Maryland, USA (Proceedings of Machine Learning Research, Vol. 162)*, Kamalika Chaudhuri, Stefanie Jegelka, Le Song, Csaba Szepesvári, Gang Niu, and Sivan Sabato (Eds.). PMLR, 23341–23362. https://proceedings.mlr.press/v162/wang22am.html

[56] Yu Wang and Tyler Derr. 2021. Tree Decomposed Graph Neural Network. In *CIKM '21: The 30th ACM International Conference on Information and Knowledge Management, Virtual Event, Queensland, Australia, November 1 - 5, 2021*. ACM, 2040–2049.

[57] Yunhai Wang, Yanyan Wang, Yinqi Sun, Lifeng Zhu, Kecheng Lu, Chi-Wing Fu, Michael Sedlmair, Oliver Deussen, and Baoquan Chen. 2017. Revisiting stress majorization as a unified framework for interactive constrained graph visualization. *IEEE transactions on visualization and computer graphics* 24, 1 (2017), 489–499.

[58] Yuelin Wang, Kai Yi, Xinliang Liu, Yu Guang Wang, and Shi Jin. 2023. ACMP: Allen-Cahn Message Passing with Attractive and Repulsive Forces for Graph Neural Networks. In *The Eleventh International Conference on Learning Representations*.

[59] Felix Wu, Amauri Souza, Tianyi Zhang, Christopher Fifty, Tao Yu, and Kilian Weinberger. 2019. Simplifying Graph Convolutional Networks. In *Proceedings of the 36th International Conference on Machine Learning*. PMLR, 6861–6871.

[60] Shu Wu, Yuyuan Tang, Yanqiao Zhu, Liang Wang, Xing Xie, and Tieniu Tan. 2019. Session-Based Recommendation with Graph Neural Networks. In *The Thirty-Third AAAI Conference on Artificial Intelligence, AAAI 2019, The Thirty-First Innovative Applications of Artificial Intelligence Conference, IAAI 2019, The Ninth AAAI Symposium on Educational Advances in Artificial Intelligence, EAAI 2019, Honolulu, Hawaii, USA, January 27 - February 1, 2019*. AAAI Press, 346–353. https://doi.org/10.1609/aaai.v33i01.3301346

[61] Keyulu Xu, Weihua Hu, Jure Leskovec, and Stefanie Jegelka. 2019. How Powerful are Graph Neural Networks?. In *7th International Conference on Learning Representations, ICLR 2019, New Orleans, LA, USA, May 6-9, 2019*. OpenReview.net. https://openreview.net/forum?id=ryGs6iA5Km

[62] Liang Yang, Mengzhe Li, Liyang Liu, Bingxin Niu, Chuan Wang, Xiaochun Cao, and Yuanfang Guo. 2021. Diverse Message Passing for Attribute with Heterophily. In *Advances in Neural Information Processing Systems 34: Annual Conference on Neural Information Processing Systems 2021, NeurIPS 2021, December 6-14, 2021, virtual*, Marc'Aurelio Ranzato, Alina Beygelzimer, Yann N. Dauphin, Percy Liang, and Jennifer Wortman Vaughan (Eds.). 4751–4763. https://proceedings.neurips.cc/paper/2021/hash/253614bbac999b38b5b60cae531c4969-Abstract.html

[63] Yongyi Yang, Tang Liu, Yangkun Wang, Jinjing Zhou, Quan Gan, Zhewei Wei, Zheng Zhang, Zengfeng Huang, and David Wipf. 2021. Graph Neural Networks Inspired by Classical Iterative Algorithms. In *Proceedings of the 38th International Conference on Machine Learning, ICML 2021, 18-24 July 2021, Virtual Event (Proceedings of Machine Learning Research, Vol. 139)*, Marina Meila and Tong Zhang (Eds.). PMLR, 11773–11783. http://proceedings.mlr.press/v139/yang21g.html

[64] Zhilin Yang, William W. Cohen, and Ruslan Salakhutdinov. 2016. Revisiting Semi-Supervised Learning with Graph Embeddings. In *Proceedings of the 33nd International Conference on Machine Learning, ICML 2016, New York City, NY, USA, June 19-24, 2016 (JMLR Workshop and Conference Proceedings, Vol. 48)*, Maria-Florina Balcan and Kilian Q. Weinberger (Eds.). JMLR.org, 40–48. http://proceedings.mlr.press/v48/yanga16.html

[65] Rex Ying, Ruining He, Kaifeng Chen, Pong Eksombatchai, William L. Hamilton, and Jure Leskovec. 2018. Graph Convolutional Neural Networks for Web-Scale Recommender Systems. In *Proceedings of the 24th ACM SIGKDD International Conference on Knowledge Discovery & Data Mining, KDD 2018, London, UK, August 19-23, 2018*, Yike Guo and Faisal Farooq (Eds.). ACM, 974–983. https://doi.org/10.1145/3219819.3219890

[66] Jiong Zhu, Yujun Yan, Lingxiao Zhao, Mark Heimann, Leman Akoglu, and Danai Koutra. 2020. Beyond Homophily in Graph Neural Networks: Current Limitations and Effective Designs. *Advances in Neural Information Processing Systems* 33 (2020).

A PROOF OF THEOREM 3.7

Proof. We will prove this theorem in three parts.

- $\mathrm{Iso}(n,d;V^2) \leq \mathrm{Iso}(n,d;E)$. It is evident that every congruent transformation $\mathcal{T} \in \mathrm{Iso}(n,d;V^2)$ is also equivalent, meaning $\mathcal{T} \in \mathrm{Iso}(n,d;E)$, since $E \subseteq V^2$.
- $\mathrm{E}(d) \leq \mathrm{Iso}(n,d;V^2)$. For an orthogonal matrix $\boldsymbol{Q}$, we can verify that
$$(\boldsymbol{Z}\boldsymbol{Q})(\boldsymbol{Z}\boldsymbol{Q})^\top = \boldsymbol{Z}\boldsymbol{Q}\boldsymbol{Q}^\top\boldsymbol{Z}^\top = \boldsymbol{Z}\boldsymbol{Z}^\top,$$
which implies $M(\boldsymbol{Z}) = M(\boldsymbol{Z}\boldsymbol{Q})$. For a translation vector $\boldsymbol{s} \in \mathbb{R}^d$, we can verify that for all $i,j \in \{1,2,\cdots,n\}$,
$$M(\boldsymbol{Z}+\boldsymbol{1}_n\boldsymbol{s}^\top)_{ij} = \|(\boldsymbol{Z}_{i:}+\boldsymbol{s}^\top)-(\boldsymbol{Z}_{j:}+\boldsymbol{s}^\top)\|_2 = M(\boldsymbol{Z})_{ij},$$
hence $M(\boldsymbol{Z}+\boldsymbol{1}_n\boldsymbol{s}^\top) = M(\boldsymbol{Z})$. Therefore, for any $\mathcal{T} \in \mathrm{E}(d)$, we have
$$M(\mathcal{T}(\boldsymbol{Z})) = M(\boldsymbol{Z}\boldsymbol{Q}+\boldsymbol{1}_n\boldsymbol{s}^\top) = M(\boldsymbol{Z}),$$
which means $\mathcal{T} \in \mathrm{Iso}(n,d;V^2)$.
- $\mathrm{Iso}(n,d;V^2) \leq \mathrm{E}(d)$. Suppose we have two embeddings $\boldsymbol{X} \in \mathbb{R}^{n\times d}$ and $\boldsymbol{Y} = \mathcal{T}(\boldsymbol{X})$ for some $\mathcal{T} \in \mathrm{Iso}(n,d;V^2)$. We need to demonstrate that $\mathcal{T}'$ can be expressed as is the composition of an orthogonal transformation and a translation transformation.
First, we translate $\boldsymbol{X}_{1:}$ and $\boldsymbol{Y}_{1:}$ to the origin by defining $\boldsymbol{X}' = \boldsymbol{X}-\boldsymbol{1}_n\boldsymbol{X}_{1:}$ and $\boldsymbol{Y}' = \boldsymbol{Y}-\boldsymbol{1}_n\boldsymbol{Y}_{1:}$. The metric matrix is preserved under translation, i.e., $M(\boldsymbol{Y}') = M(\boldsymbol{Y}) = M(\boldsymbol{X}) = M(\boldsymbol{X}')$. Now, for $i \in \{1,2,\cdots,n\}$, we have
$$\|\boldsymbol{X}'_{i:}\| = \|\boldsymbol{X}'_{i:}-\boldsymbol{0}\| = \|\boldsymbol{X}'_{i:}-\boldsymbol{X}'_{1:}\| = M(\boldsymbol{X}')_{i1} = M(\boldsymbol{Y}')_{i1}.$$
For $\boldsymbol{Y}'$, we have:
$$\|\boldsymbol{Y}'_{i:}\| = M(\boldsymbol{Y}')_{i1}.$$
Let us denote $\boldsymbol{Y}'$ as $\boldsymbol{Y}' = \mathcal{T}'(\boldsymbol{X}')$, and we will now show that $\mathcal{T}'$ is an orthogonal transformation.
We first show that $\mathcal{T}'$ preserves the inner product, i.e., $\boldsymbol{Y}'(\boldsymbol{Y}')^\top = \boldsymbol{X}'(\boldsymbol{X}')^\top$. Note that for $i,j \in \{1,2,\cdots,n\}$, we have
$$\begin{aligned}\boldsymbol{X}'^\top_{i:}\boldsymbol{X}'_{j:} &= \frac{1}{2}(\|\boldsymbol{X}'_{i:}\|^2+\|\boldsymbol{X}'_{j:}\|^2-\|\boldsymbol{X}'_{i:}-\boldsymbol{X}'_{j:}\|^2)\\ &= \frac{1}{2}(M(\boldsymbol{X}')_{i1}+M(\boldsymbol{X}')_{j1}-M(\boldsymbol{X}')_{ij}),\end{aligned} \tag{17}$$
and similarly,
$$\begin{aligned}\boldsymbol{Y}'^\top_{i:}\boldsymbol{Y}'_{j:} &= \frac{1}{2}(\|\boldsymbol{Y}'_{i:}\|^2+\|\boldsymbol{Y}'_{j:}\|^2-\|\boldsymbol{Y}'_{i:}-\boldsymbol{Y}'_{j:}\|^2)\\ &= \frac{1}{2}(M(\boldsymbol{Y}')_{i1}+M(\boldsymbol{Y}')_{j1}-M(\boldsymbol{Y}')_{ij}).\end{aligned} \tag{18}$$
Since $M(\boldsymbol{X}') = M(\boldsymbol{Y}')$, we have $\left((\boldsymbol{Y}')(\boldsymbol{Y}')^\top\right)_{ij} = \boldsymbol{Y}'_{i:}(\boldsymbol{Y}')^\top_{j:} = \boldsymbol{X}'_{i:}(\boldsymbol{X}'_{j:})^\top = \left((\boldsymbol{X}')(\boldsymbol{X}')^\top\right)_{ij}$, thus $\boldsymbol{Y}'(\boldsymbol{Y}')^\top = \boldsymbol{X}'(\boldsymbol{X}')^\top$.
We then demonstrate that $\mathcal{T}'$ is linear. For any vector $\boldsymbol{x}$, $\boldsymbol{y} \in \mathbb{R}^d$ and scalars a, b in $\mathbb{R}$, let $\boldsymbol{z} = \mathcal{T}'(a\boldsymbol{x}+b\boldsymbol{y})-a\mathcal{T}'(\boldsymbol{x})-b\mathcal{T}'(\boldsymbol{y})$. We can then verify that $\boldsymbol{z}^\top\boldsymbol{z} = 0$ through some calculations:
$$\begin{aligned}\boldsymbol{z}^\top\boldsymbol{z} = {}&\mathcal{T}'(a\boldsymbol{x}+b\boldsymbol{y})^\top\mathcal{T}'(a\boldsymbol{x}+b\boldsymbol{y})+a^2\mathcal{T}'(\boldsymbol{x})^\top\mathcal{T}'(\boldsymbol{x})\\ &+b^2\mathcal{T}'(\boldsymbol{y})^\top\mathcal{T}'(\boldsymbol{y})-2a\mathcal{T}'(a\boldsymbol{x}+b\boldsymbol{y})^\top\mathcal{T}'(\boldsymbol{x})\\ &-2b\mathcal{T}'(a\boldsymbol{x}+b\boldsymbol{y})^\top\mathcal{T}'(\boldsymbol{y})+2ab\mathcal{T}'(\boldsymbol{x})^\top\mathcal{T}'(\boldsymbol{y})\\ = {}&(a\boldsymbol{x}+b\boldsymbol{y})^\top(a\boldsymbol{x}+b\boldsymbol{y})+a^2\boldsymbol{x}^\top\boldsymbol{x}+b^2\boldsymbol{y}^\top\boldsymbol{y}\\ &-2a(a\boldsymbol{x}+b\boldsymbol{y})^\top\boldsymbol{x}-2b(a\boldsymbol{x}+b\boldsymbol{y})^\top\boldsymbol{y}+2ab\boldsymbol{x}^\top\boldsymbol{y}\\ = {}&2a^2\boldsymbol{x}^\top\boldsymbol{x}+2b^2\boldsymbol{y}^\top\boldsymbol{y}+2ab\boldsymbol{x}^\top\boldsymbol{y}\\ &-2a^2\boldsymbol{x}^\top\boldsymbol{x}-2ab\boldsymbol{x}^\top\boldsymbol{y}-2ab\boldsymbol{x}^\top\boldsymbol{y}-2b^2\boldsymbol{y}^\top\boldsymbol{y}+2ab\boldsymbol{x}^\top\boldsymbol{y}\\ = {}&0.\end{aligned}$$
Consequently, we find that $\boldsymbol{z} = \boldsymbol{0}$, which implies $\mathcal{T}'(a\boldsymbol{x}+b\boldsymbol{y}) = a\mathcal{T}'(\boldsymbol{x})+b\mathcal{T}'(\boldsymbol{y})$. Therefore, the mapping $\mathcal{T}'$ is linear. Since $\mathcal{T}'$ is linear, it can be represented by a matrix $\boldsymbol{Q}$ (with respect to the standard orthonormal basis), such that $\mathcal{T}'(\boldsymbol{x}) = \boldsymbol{Q}\boldsymbol{x}$. Hence, $\|\mathcal{T}'(\boldsymbol{x})\| = \|\boldsymbol{x}\|$ if and only if $(\boldsymbol{Q}\boldsymbol{x})^\top\boldsymbol{Q}\boldsymbol{x} = \boldsymbol{x}^\top\boldsymbol{x}$, which further leads to $\boldsymbol{Q}^\top\boldsymbol{Q} = \boldsymbol{I}$. From this, we can conclude that $\mathcal{T}'$ is an orthogonal transformation.
Therefore, $\mathcal{T}(\boldsymbol{X}) = \boldsymbol{Q}(\boldsymbol{X}-\boldsymbol{1}_n\boldsymbol{X}_{1:})+\boldsymbol{1}_n\boldsymbol{Y}_{1:} = \boldsymbol{Q}\boldsymbol{X}-\boldsymbol{Q}\boldsymbol{1}_n\boldsymbol{X}_{1:}+\boldsymbol{1}_n\boldsymbol{Y}_{1:}$, which implies $\mathcal{T} \in \mathrm{E}(d)$.

This concludes the proof. □

B PROOF OF THEOREM 4.1

Proof. Since the composition of orthogonal and translation transformations are the only types of congruent transformations in $\mathbb{R}^d$ (according to Theorem 3.7), we can express $\boldsymbol{Z}_2$ as $\boldsymbol{Z}_2 = \boldsymbol{Z}_1\boldsymbol{Q}+\boldsymbol{1}_n\boldsymbol{s}^\top$, where $\boldsymbol{Q} \in \mathrm{O}(d)$ is an orthogonal matrix, $\boldsymbol{1}_n \in \mathbb{R}^n$ is an all-one vector, and $\boldsymbol{s} \in \mathbb{R}^d$ is a translation vector. Thus, for any MLP_M with parameters $\boldsymbol{W}_M^{(0)},\cdots,\boldsymbol{W}_M^{(L-1)}$ and $\boldsymbol{b}_M^{(0)},\cdots,\boldsymbol{b}_M^{(L-1)}$, we can construct another MLP_N with parameters $\boldsymbol{W}_N^{(0)},\boldsymbol{W}_M^{(1)}\cdots,\boldsymbol{W}_M^{(L-1)}$ and $\boldsymbol{b}_N^{(0)},\boldsymbol{b}_M^{(1)}\cdots,\boldsymbol{b}_M^{(L-1)}$, where $\boldsymbol{W}_N^{(0)} = \boldsymbol{Q}^{-1}\boldsymbol{W}_M^{(0)}$ and $\boldsymbol{b}_N^{(0)} = \boldsymbol{b}_M^{(0)}-(\boldsymbol{Q}^{-1}\mathbf{W}_M^{(0)})^\top\boldsymbol{s}$. It is easy to verify that $\mathrm{MLP}_M(\boldsymbol{Z}_1) = \mathrm{MLP}_N(\boldsymbol{Z}_2)$, and the theorem follows. □

C PROOF OF THEOREM 5.1

Proof. Expanding the left side of the equation and using the definition of $\mathrm{Iso}(E)$, we have:
$$\begin{aligned}E_p(\sigma(\boldsymbol{Z});\boldsymbol{M},E) &= \sum_{(i,j)\in E}\frac{1}{2}\left(\left\|\sigma(\boldsymbol{Z})_{i:}-\sigma(\boldsymbol{Z})_{j:}\right\|_2-\boldsymbol{M}_{ij}\right)^2\\ &= \sum_{(i,j)\in E}\frac{1}{2}\left(\left\|\boldsymbol{Z}_{i:}-\boldsymbol{Z}_{j:}\right\|_2-\boldsymbol{M}_{ij}\right)^2\\ &= E_p(\boldsymbol{Z};\boldsymbol{M},E).\end{aligned}$$
Therefore, the theorem follows. □

D VISUALIZATION RESULTS OF SGC AND APPNP

We present the visualization results of the SGC layers (Figure 8 and Figure 9) and APPNP layers (Figure 10 and Figure 11) for the two synthetic graphs described earlier.

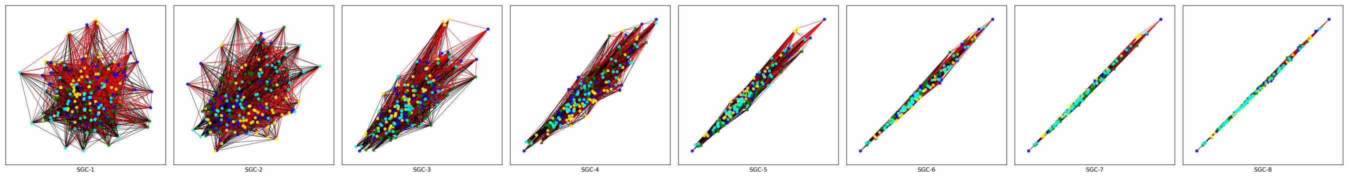

Figure 8: The results of the homophilic SBM graph of SGC layers.

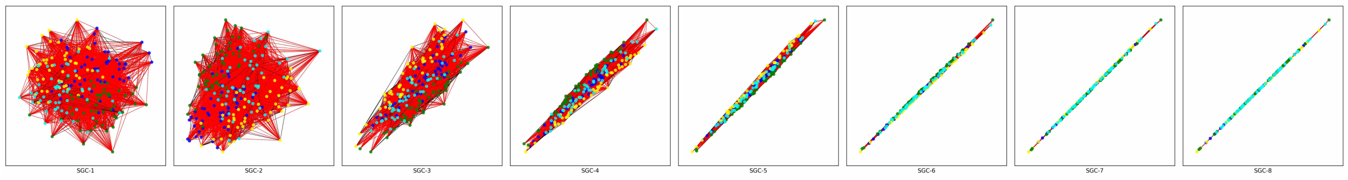

Figure 9: The results of the heterophilic SBM graph of SGC layers.

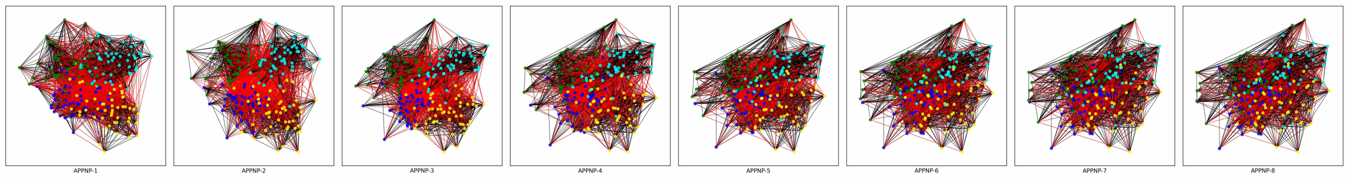

Figure 10: The results of the homophilic SBM graph of APPNP layers.

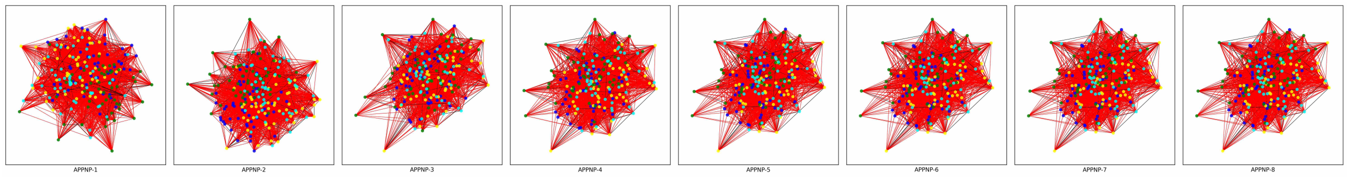

Figure 11: The results of the heterophilic SBM graph of APPNP layers.

E GRAPH REGRESSION

Settings. We utilized the publicly available train/validation/test split provided by the PyTorch Geometric Library. For all datasets, we set the number of hidden units to 64. Subsequently, we conduct hyperparameter tuning for each model on each dataset by employing the TPESampler from the optuna package. This process is repeated 100 times. Below, we present the ranges of the hyperparameters:

- `learning_rate` for all models: {1e-3, 5e-3, 1e-2, 5e-2};
- `weight_decay` for all models: {0.0, 1e-5, 5e-5, 1e-4, 5e-4, 1e-3, 5e-3, 1e-2};
- `dropout` for all models: {0.0, 0.1, 0.3, 0.5};
- `num_layers` for all models: {2, 4, 8};
- `alpha` for MGNN: {0.00, 0.01, $\cdots$, 0.99, 1.00};
- `beta` for MGNN: {0.00, 0.01, $\cdots$, 0.99, 1.00};
- `theta` for MGNN: {0.5, 1.0, 1.5};
- `initial`: for MGNN: {'Linear', 'MLP'};
- `attention` for MGNN: {'concat', 'bilinear'}.

Due to limited experiment time, we limit the training of each model to a maximum of 500 epochs. A batch size of 512 is utilized, and early stopping is implemented after 50 epochs on each dataset. Following hyperparameter tuning, we report the results. To enhance reliability, we repeat this process five times and calculat the mean MAE (Mean Absolute Error) and standard deviation for each model.

Analysis of the Results. We observed in our experiments that our MGNN model generally required more epochs to converge better, so the small epochs and insufficient training may have hindered its performance. In addition, although the GIN model outperforms other models under our graph regression experiment setting, it generally performs poorly in the node classification task. Therefore, our MGNN model has better overall performance than the GIN model. It is also important to emphasize that our MGNN model only relies on the **partial** metric information defined on the edges, so it cannot be directly compared to those transformers or global GNNs that utilize the full (global or all-pair) metric information.